Draft version January 14, 2013
Preprint typeset using LaTeX style emulateapj v. 11/10/09

arXiv:1103.1890v1 [astro-ph.CO] 9 Mar 2011

PROBING THE IGM/GALAXY CONNECTION IV: THE LCO/WFCCD GALAXY SURVEY OF 20 FIELDS SURROUNDING UV BRIGHT QUASARS

J. Xavier Prochaska[1], B. Weiner[2], H.-W. Chen[3], K.L. Cooksey[4], J.S. Mulchaey[5],

Draft version January 14, 2013

ABSTRACT

We publish the survey for galaxies in 20 fields containing ultraviolet bright quasars (with $z_{\rm em} \approx 0.1$ to 0.5) that can be used to study the association between galaxies and absorption systems from the low-z intergalactic medium (IGM). The survey is magnitude limited ($R \approx 19.5$ mag) and highly complete out to $10'$ from the quasar in each field. It was designed to detect dwarf galaxies ($L \approx 0.1L^*$) at an impact parameter $\rho \approx 1$ Mpc ($z = 0.1$) from a quasar. The complete sample (all 20 fields) includes R-band photometry for 84718 sources and confirmed redshifts for 2800 sources. This includes 1198 galaxies with $0.005 < z < (z_{\rm em} - 0.01)$ at a median redshift of 0.18, which may associated with IGM absorption lines. All of the imaging was acquired with cameras on the Swope $40''$ telescope and the spectra were obtained via slitmask observations using the WFCCD spectrograph on the Dupont $100''$ telescope at Las Campanas Observatory (LCO). This paper describes the data reduction, imaging analysis, photometry, and spectral analysis of the survey. We tabulate the principal measurements for all sources in each field and provide the spectroscopic dataset online.

Subject headings: IGM : metals, O VI, galaxies—techniques

1. INTRODUCTION

The intergalactic medium (IGM) is the gas and dust which permeates the space between galaxies in our universe. The IGM is inferred to be the dominant repository of baryons in our universe; it provides the fuel for galaxies and serves as a 'sink' for the metals they expel. The IGM is almost exclusively observed through absorption-line techniques in the spectra of distant objects, e.g. quasars, gamma-ray bursts. The so-called Lyα forest, for example, is the thicket of H I absorption lines which trace modest overdensities in the universe.

Despite its name, which suggests a disconnect from galaxies, the IGM exhibits several characteristics which connect it to them. Chief among these is the presence of metals, generally in the form of highly-ionized species like C IV, Si IV, and O VI absorption. The medium is too diffuse and ionized to support *in situ* star-formation, therefore it is expected that these metals were produced within galaxies and transported by one or more mechanisms to the IGM (e.g. galactic-scale winds, tidal stripping). Identifying the timing, the processes, and the precise interplay between galaxies and the IGM remains a very active area of current astrophysical research (e.g. Scannapieco et al. 2006; Oppenheimer & Davé 2009; Wiersma et al. 2010).

For several decades now, researchers have surveyed the fields surrounding bright quasars with the goal of connecting galaxies that they discover to specific characteristics of the IGM (as revealed by rest-frame UV spectroscopy of the quasars). These include surveys to explore the association of galaxies to the Lyα forest (Morris et al. 1993; Lanzetta et al. 1995; Stocke et al. 1995; Shull et al. 1996; Bowen et al. 2002; Chen et al. 2005; Shone et al. 2010); searches for galaxies related to strong Mg II lines (Bergeron & Boisse 1991; Steidel 1993; Barton & Cooke 2009; Chen et al. 2010); and studies of the structures giving rise to O VI absorption (Tripp & Savage 2000; Bowen et al. 2001; Savage et al. 2002; Sembach et al. 2004; Tumlinson et al. 2005; Prochaska et al. 2006; Stocke et al. 2006; Tripp et al. 2006; Cooksey et al. 2008; Chen & Mulchaey 2009; Wakker & Savage 2009). The latter ion has received considerable attention because it has been proposed to trace the $T \approx 10^{5-7}$ K phase of the IGM, termed the warm-hot intergalactic medium (WHIM). Although the WHIM is a generic prediction of cosmological simulations (Cen & Ostriker 1999; Davé et al. 2001; Fang & Bryan 2001), its low density and modest temperature make it especially elusive to empirical detection. The O VI doublet, however, has been extensively surveyed and owing to its high ionization state may track a portion of the WHIM.

Motivated by the analysis of O VI and its relation to galaxies and the WHIM, we initiated a program to survey galaxies in the fields surrounding UV-bright, $z_{\rm em} \gtrsim 0.1$ quasars that were targeted (or likely to be targeted) by the *Far Ultraviolet Spectroscopic Explorer (FUSE)* and/or the *Hubble Space Telescope (HST)*. Prior to the commissioning of the Cosmic Origins Spectrograph (COS), there were only a small set of known quasars that were bright enough for such observations. The sources are widely separated across the sky such that existing, ongoing, and/or planned galaxy surveys (e.g. SDSS, 2dF) do not cover the fields or are often too shallow for studying $L > L^*$ galaxies beyond $z \approx 0.05$.

[1] Department of Astronomy and Astrophysics & UCO/Lick Observatory, University of California, 1156 High Street, Santa Cruz, CA 95064; xavier@ucolick.org
[2] Steward Observatory, University of Arizona, 933 N. Cherry Ave., Tucson, AZ 85721; bjw@as.arizona.edu
[3] Department of Astronomy; University of Chicago; 5640 S. Ellis Ave., Chicago, IL 60637; hchen@oddjob.uchicago.edu
[4] NSF Astronomy & Astrophysics Postdoctoral Fellow, MIT Kavli Institute for Astrophysics & Space Research, 77 Massachusetts Avenue, 37-611, Cambridge, MA 02139, USA; kcooksey@space.mit.edu
[5] Carnegie Observatories; 213 Santa Barbara St., Pasadena, CA 91101; mulchaey@obs.carnegiescience.edu

TABLE 1
Summary of Fields Surveyed

Quasar	RA (J2000)	DEC (J2000)	$z_{\rm em}$	*HST* UV Spectroscopic Datasets	*FUSE*[a]	$R_{\rm max}$	$N^b_{\rm spec}$	$C^{5'}_{19.5}$	$C^{10'}_{19.5}$
Q0026+1259	00:29:13.8	+13:16:04	0.142	GHRS/(G270M)	20	20.0	60	100	91
Ton S 180	00:57:20.0	–22:22:56	0.062	STIS/(G140M,G230MB)	132	19.7	7	100	93
Ton S 210	01:21:51.5	–28:20:57	0.116	STIS/(E140M,E230M)	57	20.0	7	86	90
PKS0312-77	03:11:55.2	–76:51:51	0.223	STIS/(E140M)		20.0	56	100	97
PKS0405-123	04:07:48.4	–12:11:37	0.573	STIS/(E140M,G230M); GHRS/(G160M,G200M)	71	20.0	565	100	97
PKS0558-504	05:59:47.4	–50:26:52	0.137	STIS/(G230MB)	400	20.0	16	100	99
PG1004+130	10:07:26.1	+12:48:56	0.240	STIS/(G140M)	85	19.5	61	74	71
HE1029-140	10:31:54.3	–14:16:51	0.086	STIS/(G140M)		19.8	8	100	95
PG1116+215	11:19:08.7	+21:19:18	0.176	STIS/(G140M,E140M,E230M); GHRS/(G140L)	76	20.0	74	76	79
PG1211+143	12:14:17.7	+14:03:13	0.081	STIS/(G140M,E140M); GHRS/(G140L,G270M)	52	19.5	25	61	56
PG1216+069	12:19:20.9	+06:38:38	0.331	STIS/(E140M); GHRS/(G140L)	13	20.0	101	100	89
3C273	12:29:6.70	+02:03:09	0.158	STIS/(E140M); GHRS/(FG130,FG190,G160M)	42	20.0	32	81	84
Q1230+0947	12:33:25.8	+09:31:23	0.415	GHRS/(G140L)	13	19.5	99	83	77
PKS1302-102	13:05:33.0	–10:33:19	0.286	STIS/(E140M)	140	19.5	63	89	65
PG1307+085	13:09:47.0	+08:19:49	0.155	STIS/(G230MB)	11	19.5	41	79	75
MRK1383	14:29:06.4	+01:17:06	0.086	STIS/(E140M,G140M)	64	19.5	5	79	68
Q1553+113	15:55:43.0	+11:11:24	0.360		20	20.0	106	90	85
PKS2005-489	20:09:25.4	–48:49:54	0.071	STIS/(G140M)	48	20.0	32	97	97
FJ2155-0922	21:55:01.5	–09:22:25	0.192	STIS/(E140M,G230MB)	46	20.0	105	100	95
PKS2155-304	21:58:51.8	–30:13:30	0.116	STIS/(E140M); GHRS/(G160M,ECH-B,G140L)	123	20.0	43	96	96

Note. — Columns 9 and 10 list the completeness percent of the spectroscopic survey in each field to $R = 19.5$ mag for a radius of 5 and 10 arcminutes respectively.

[a] Total integration time in ks.

[b] Number of spectroscopically determined galaxy redshifts for objects with $0.005 < z < z_{\rm em}$.

Therefore, we designed a survey with two main observational goals: (1) achieve high completeness for galaxies as faint as $\approx 0.1L^*$ at $z = 0.1$; and (2) survey an area corresponding to at least 1 Mpc at $z = 0.1$. Technically, this implied a magnitude limit of $R \approx 19.5$ mag and a field-of-view (FOV) of roughly $10'$ radius around each quasar. These requirements were well-suited to the WFCCD spectrograph on the $100''$ Dupont Telescope at Las Campanas Observatory (LCO). Over the course of several years, we targeted 20 fields at equatorial and Southern declinations (Table 1). Early results from this survey have been used to explore the IGM/galaxy connection for O VI absorbers (Prochaska et al. 2006; Cooksey et al. 2008), the Lyα forest (Chen et al. 2005), and a Lyman limit absorber (Lehner et al. 2009).

With this paper, we provide the full data release of the LCO/WFCCD survey. This stands, for now, as the largest dataset for exploring the association between the IGM and galaxies and their large-scale structures at $z \sim 0.1$. This manuscript comments on galaxies derived only from our own LCO/WFCCD survey and we emphasize that other datasets (e.g. SDSS) and publications do provide complementary coverage for about half of the fields. In future (and previous) papers, we analyze the IGM/galaxy connection with this dataset. We organize the paper as follows: § 2 describes the observations, data reduction, and spectral analysis for redshift determinations; we present our survey of the fields in § 3; and offer a brief summary in § 4. Unless otherwise specified, we adopt the 5yr WMAP cosmology (Dunkley et al. 2009): $\Omega_\Lambda = 0.74, \Omega_m = 0.26, H_0 = 72\,{\rm km\,s^{-1}\,Mpc^{-1}}$. Furthermore, all distances are quoted in proper units unless otherwise denoted.

2. OBSERVATIONS AND DATA REDUCTION

We selected 20 fields accessible from Las Campanas Observatory (declination $\delta < 25$ deg) surrounding UV bright quasars with emission redshifts $z_{\rm em} > 0.05$. These quasars had existing UV spectroscopy from the *HST* or *FUSE* telescopes, had planned UV spectroscopic observations with one of these telescopes, and/or have sufficiently high UV flux to permit UV spectroscopic observations with one of these facilities. The quasars were also chosen to have a wide range of right ascension, to enable a year-round observing campaign. The quasars and their UV spectroscopic datasets are summarized in Table 1.

All of the fields in our survey were imaged with the Swope $40''$ telescope using a direct imaging camera. The majority were taken with the SITe1 CCD which has $0.6964''$ pixels in a 2048×2048 array. The remainder were observed with the SITe3 CCD which has $0.435''$ pixels in a 2048×3150 array. All of the fields were imaged through an R-band filter and most also had contemporaneous B-band images taken. The data were obtained in a series of dithered exposures intended to map at least a $20' \times 20'$ field-of-view (FOV). This was designed to enable a survey to approximately a 1 Mpc impact parameter ρ at $z \approx 0.1$. Most of the imaging data were obtained under photometric conditions; Table 2 summarizes the weather and provides a log of the observations. Most of the data were acquired in good seeing conditions, i.e. FWHM $\approx 1''$.

The imaging data were reduced with standard IRAF routines to overscan subtract and flat-field the images. We used custom routines to determine integer offsets between the dithered images and combined the frames after weighting by a global measure of the inverse variance. We derived a photometric solution for each night from analysis of Landoldt standard stars (Landolt 1992) that were observed at a range of airmass. We solved for the zeropoint, airmass and $(B-R)$ color terms. We estimate the systematic uncertainty related to the photometric solution to be approximately 0.05 mag.

TABLE 2
Log of Imaging Observations

Field	UT Date	CCD	Filter	Exp.	Conditions
Q0026+1259	26 Oct 2000	SITe1	B	2x450s	Photometric
			R	3x600s	Photometric
Q0046+112	26 Oct 2000	SITe1	B	2x450s	Photometric
			R	3x600s	Photometric
Ton S 180	26 Oct 2000	SITe1	B	2x450s	Photometric
			R	3x600s	Photometric
HE0153−4520	14 Sep 2001	SITe3	B	5x450s	Photometric
			R	6x600s	Photometric
Ton S 210	26 Oct 2000	SITe1	B	2x450s	Photometric
			R	3x600s	Photometric
	02 Oct 2002	SITe3	R	12x600s	Cirrus
	03 Oct 2002	SITe3	R	9x600s	
	04 Oct 2002	SITe3	R	13x600s	
PKS0312−770	02 Oct 2002	SITe3	R	6x450s	Cirrus
	04 Oct 2002	SITe3	R	3x600s	
PKS0405−123	26 Oct 2000	SITe1	B	2x450s	Windy, photometric
			R	5x600s	Windy, photometric
	03 Oct 2002	SITe3	R	18x600s	
	04 Oct 2002	SITe3	R	16x600s	
HE0450−2958	26 Feb 2001	SITe1	B	2x450s	Photometric
			R	3x600s	Photometric
AKN 120	23 Feb 2001	SITe1	B	2x450s	Photometric
			R	4x600s	Photometric
PKS0558−504	26 Oct 2000	SITe1	B	2x450s	Windy, photometric
			R	4x600s	Windy, photometric
B0736+017	21 Feb 2001	SITe1	B	2x450s	Photometric
			R	4x600s	Photometric
PG0832+25	26 Feb 2001	SITe1	B	2x450s	Photometric
			R	3x600s	Photometric
IR0914−6206	21 Feb 2001	SITe1	B	2x450s	Photometric
			R	3x600s	Photometric
PG1001+054	24 Feb 2001	SITe1	B	2x450s	Photometric
			R	4x600s	Photometric
PG1004+130	24 Feb 2001	SITe1	B	2x500s	Photometric
			R	4x600s	Photometric
PG1011−040	24 Feb 2001	SITe1	B	2x450s	Photometric
			R	3x600s	Photometric
HE1015−1618	27 Feb 2001	SITe1	B	2x450s	Photometric
			R	3x600s	Photometric
HE1029−140	23 Feb 2001	SITe1	B	2x500s	Photometric
			R	3x600s	Photometric
	08 Apr 2003	SITe3	B	13x600s	Cirrus
HE1050−2711	28 Feb 2001	SITe1	B	2x450s	Photometric
			R	3x600s	Photometric
HE1115−1735	27 Feb 2001	SITe1	B	2x450s	Photometric
			R	3x600s	Photometric
PG1116+215	21 Feb 2001	SITe1	B	3x600s	Photometric
			R	6x600s	Photometric
	23 Feb 2001		B	3x600s	Photometric
			R	3x600s	Photometric
HE1122−1649	23 Feb 2001	SITe1	B	2x500s	Photometric
			R	3x600s	Photometric
MRK 1298	07 Apr 2002	SITe3	B	6x600s	Photometric
			R	12x600s	Photometric
PG1126+215	25 Feb 2001	SITe1	R	7x600s	Photometric
PG1211+143	09 Apr 2002	SITe3	B	6x600s	Photometric
			R	14x600s	Photometric
PG1216+069	25 Feb 2001	SITe1	B	2x600s	Photometric
			R	4x600s	Photometric
	26 Feb 2001		B	4x600s	Photometric
			R	7x600s	Photometric

Note. — [The complete version of this table is in the electronic edition of the Journal. The printed edition contains only a sample.]

TABLE 3
Log of WFCCD Observations

Field	UT Date	Mask	Exp.	Conditions
Q0026+1259	31 Oct 2002	M1	3600	Clear
	01 Nov 2002	M2	3600	Clear
	02 Nov 2002	M3	3600	Clear
	03 Nov 2002	M4	3600	Clear
	04 Nov 2002	M5	3600	Clear
	05 Nov 2002	M6	1800	Clear
	06 Nov 2002	M6	1800	Clear
Ton S 180	10 Sep 2001	M1	5400	Photometric
	12 Sep 2001	M2	7200	Clear, poor seeing
	14 Sep 2001	M3	3600	Clear
	15 Sep 2001	M4	3600	Clear
	16 Sep 2001	M5	3600	Clear
Ton S 210	12 Sep 2001	M1	5400	Cirrus
	13 Sep 2001	M2	3600	Clear
	13 Sep 2001	M4	3600	Clear
	14 Sep 2001	M3	3600	Clear
PKS0312−770	01 Nov 2002	M1	3600	Clear
	01 Nov 2002	M2	3600	Clear
	02 Nov 2002	M3	3000	Clear
	03 Nov 2002	M4	3300	Clear
	04 Nov 2002	M5	3600	Clear
PKS0405−123	13 Sep 2001	M1	3600	Cirrus
	14 Sep 2001	M3	3600	Clear
	15 Sep 2001	M4	3600	Clear
	16 Sep 2001	M2	3600	Clear
	31 Oct 2002	M5	3600	Clear
	31 Oct 2002	S	1800	Clear
	02 Nov 2002	EE1	3600	Clear
	02 Nov 2002	EE2	3600	Clear
	02 Nov 2002	EE3	3000	Clear
	03 Nov 2002	NN1	3000	Clear
	03 Nov 2002	NN2	3000	Clear
	03 Nov 2002	NN3	3000	Clear
	03 Nov 2002	NN4	3300	Clear
	04 Nov 2002	WW1	3600	Clear
	04 Nov 2002	WW2	3600	Clear
	04 Nov 2002	WW3	3600	Clear
	04 Nov 2002	WW4	3600	Clear
	05 Nov 2002	SS1	4200	Clear
	05 Nov 2002	SS2	3600	Clear
	05 Nov 2002	SS3	3600	Clear
	05 Nov 2002	SS4	3600	Clear
PKS0558−504	13 Sep 2001	M1	3600	Cirrus
	14 Sep 2001	M3	3600	Clear
	15 Sep 2001	M4	3600	Clear
	16 Sep 2001	M2	3600	Clear
	31 Oct 2002	M5	4200	Clear
	01 Nov 2002	M6	3600	Clear
	01 Nov 2002	M7	1800	Clear
	02 Nov 2002	M7	1800	Clear
	06 Nov 2002	M2	1800	Clear
PG1001+054	22 Apr 2001	S0	3600	Photometric
PG1004+130	31 May 2003	M1	3600	Cirrus
	01 Jun 2003	M2	3600	Cirrus
	02 Jun 2003	M3	3600	Clear
HE1029−140	18 Apr 2001	S0	3600	Photometric
	19 Apr 2001	B0	5400	Photometric
	20 Apr 2001	B1	3600	Light cirrus
	21 Apr 2001	S1	3600	Cirrus
PG1116+215	18 Apr 2001	B0	3600	Photometric
	18 Apr 2001	B1	3600	Photometric
	19 Apr 2001	S0	5400	Photometric
	20 Apr 2001	B2	3600	Light cirrus
	22 Apr 2001	F1	3600	Photometric
	05 Jun 2003	F1	3600	Clouds
	06 Jun 2003	F1	5400	Clear
PG1211+143	31 May 2003	M2	3600	Cirrus
	01 Jun 2003	M3	3600	Cirrus
	02 Jun 2003	M1	3600	Clear
PG1216+069	03 Jun 2003	M1	5400	Clear
	03 Jun 2003	M2	5150	Cirrus
	03 Jun 2003	M3	3600	Clear
	03 Jun 2003	M4	3600	Clear
	06 Jun 2003	M2	3600	Clear

Note. — [The complete version of this table is in the electronic edition of the Journal. The printed edition contains only a sample.]

Each combined R-band image was analyzed with the SExtractor (v2.0 Bertin & Arnouts 1996) package. The parameters were set to require a minimum detection area of 6 pixels and a detection threshold of 1.5σ above the RMS of the sky background. For each object detected, SExtractor reports a star-galaxy (S/G) classifier with values ranging from 0 to 1 where unity indicates a point-spread-function consistent with a point source (i.e. a likely star). Finally, we produced a segmentation map of each field and calculated B and R magnitudes by summing the flux in the pixels assigned to each object. There are no corrections made for flux that falls below our detection threshold. The true galaxy magnitudes, therefore, may be up to a few tenths magnitude brighter especially for low-surface brightness galaxies.

Proper astrometry for each field was applied with the publicly- available Image World Coordinate Setting Program *imwcs*[6] version 3.6.8. First, several World Coordinate System (WCS) keywords were added to the reduced and combined image header in order to define its estimated pointing and plate scale ($0.6964''\,\mathrm{pix}^{-1}$ for the SITe1 CCD and $0.4349''\,\mathrm{pix}^{-1}$ for SITe3). Next, we used *imwcs* to fit a plane-tangent projection, using stars in the image that *imwcs* identified and stars from a reference catalog, namely, the US Naval Observatory astrometric catalog USNO-A2.0.[7] The *imwcs* algorithm typically matched a dozen or more stars and converged in six iterations, with a mean arcsec offset of $0.15''$ in any given image. Finally, all astrometized images were visually compared to the USNO-A2.0 sample to verify that the solution held across the whole field (e.g., no systematic rotation was obvious towards the outskirts of the image).

Based on our SExtractor analysis of the images, we designed a set of slit masks for each field to be used with the WFCCD instrument on the Dupont $100''$ telescope. Targets were identified as follows. First, we examined the isophotal area versus R magnitude from the imaging of a given field. In all cases, stars trace out a well-defined locus for $R < 19.5$ mag (see Fig. 1 of Prochaska et al. 2006, for an example). We traced this locus and discarded all objects that fall within the stellar region or fall just outside the locus and have a S/G value greater than 0.98. We also did not target the few, very bright ($R < 15$ mag) and very large (angular diameter $> 10''$) galaxies that exist in the survey fields. Most of these have previously published redshifts and/or lie at too low redshift ($z < 0.01$) for our main scientific program. For those that remained, we targeted all objects with $R \leq R_{\rm max}$ and $\theta < \theta_{\rm max}$ of the QSO. We set $R_{\rm max} \geq 19.5$ mag, adopting fainter values for fields with a lower surface density of targets on the sky or where we had particular scientific interest in the field (see Table 1). For all but two of the fields, $\theta_{\rm max} = 10'$. The two exceptions are PKS0312−770 and PKS0405−123, where we expanded the survey to cover $\theta_{\rm max} \approx 15'$ and $\approx 20'$ respectively.

We performed multi-slit spectroscopy on each field with the WFCCD spectrometer using the blue grism and the Tek#5 CCD. This affords a spectral resolution FWHM $\approx 375\mathrm{km\ s}^{-1}$, a dispersion of ≈ 2Å per pixel, and a nominal wavelength coverage $\lambda \approx 3800$–9000Å. Our standard integration was a pair of 1800s exposures, and most of the data were obtained under clear conditions. Longer total exposure times were used for the faintest fields or in worse conditions. These exposure times generally achieved a signal-to-noise S/N > 3 per pixel for even the faintest objects. Table 3 shows a log of the WFCCD observations.

All of these WFCCD data were reduced with a custom IDL software package[8] (see Prochaska et al. 2006, for a full description). The extracted and coadded 1D spectra were analyzed with a modified version of the SDSS pipeline task *zfind* to establish the object's redshift. This routine fits PCA templates derived from the SDSS dataset (Early Data Release; Stoughton et al. 2002) to the emission and/or absorption lines in the object spectrum. In general, these redshift values have uncertainties of $\sigma_z \approx 10^{-4}$ (i.e. $\sigma_v \approx 30\mathrm{km\ s}^{-1}$). Each of the fits was inspected, and, when necessary, the redshift was modified to account for an obvious failure. With few exceptions, we determined an unambiguous redshift for every object on a given mask. The exceptions include rare cases where slit design or fabrication failed (e.g. significant portions of one slit overlapped another) and also faint sources that had no obvious spectral features. This PCA analysis yields eigenvalues for the four galaxy eigenspectra fitted to our data. As in Prochaska et al. (2006), we define E_C to be the eigenvalue for the first eigenfunction (which is dominated by early-type spectral features) and L_C is the the second eigenvalue minus the sum of the third and fourth coefficients. All of the spectra are publicly available[9].

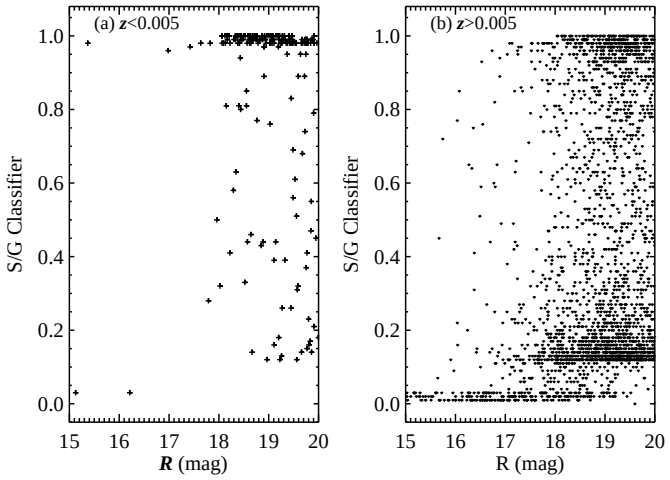


FIG. 1.— SExtractor S/G classifier as a function of the objects apparent R-band magnitude and having spectroscopic redshifts (a) $z < 0.005$ (predominantly Galactic stars) and (b) $z > 0.005$ (exclusively galaxies).

In Figure 1, we plot the S/G classifier from SExtractor for the targets with spectroscopic redshifts (a) $z < 0.005$, which are predominantly Galactic stars; and (b) $z > 0.005$, which are exclusively distant galaxies. As one expects, the majority of the $z < 0.005$ objects

[6] http://tdc-www.harvard.edu/software/wcstools/imwcs/index.html.
[7] http://tdc-www.harvard.edu/software/catalogs/ua2.html.
[8] http://www.ucolick.org/∼xavier/WFCCD/index.html
[9] http://www.ucolick.org/∼xavier/WFCCDOVI/index.html

have S/G near unity; the exceptions are primarily objects blended with some other source which was not deblended by the SExtractor algorithm. In contrast, the extragalactic sources primarily have low S/G classifiers although we note that 8% have S/G > 0.98. We caution that our targeting criteria may have missed a subset of very compact galaxies.

3. THE SURVEY FIELDS

In this section, we present the imaging data, photometry, and results from the WFCCD spectroscopy for each field. We also comment briefly on any obvious associations between the galaxies we detect and known (published) absorbers along the quasar sightlines. We stress that about half of these fields have been survey for galaxies by other efforts (e.g. SDSS). Our dicussion, however, is primarily limited to the galaxies from our LCO/WFCCD survey. Table 4 summarizes properties of the galaxies discovered in the 20 fields restricted to $0.005 < z < (z_{\rm em} + 0.01)$. Tables 5–23 summarize the photometry and spectroscopy of objects in each field.

In the following, we convert the apparent R-band magnitude of each galaxy with a measured redshift into a luminosity relative to L^*. For the latter, we adopt the Sloan r-band value from Blanton et al. (2003) as measured from the Sloan Digital Sky Survey which corresponds to $z \approx 0.1$: $r^* = -20.44 + 5\log h_{100}$. With the cosmology we have adopted, this yields $r^* = -21.12$ mag.

For each galaxy, we assess the spectral type from the E_C and L_C coefficients as follows (based in part on a visual inspection of several tens of the galaxies):

- Early-type: $E_C > 0.6$ and $L_C < 0.6$
- Late-type: $E_C < 0.8$ and $L_C > 0.4$, or $E_C < 0$ and $L_C > 0.2$, or $E_C < 0$ and $L_C < 0$.

Galaxies with any other pair of coefficient values are labelled 'unknown'. For every galaxy with an impact parameter $\rho < 300$ kpc we have visually verified each spectral type, placing each into either the late or early-type category.

We then imposed a k-correction to the apparent magnitude using a redshifted template spectrum integrated with an R-band filter. We use an E/S0 template for the early-type galaxies, and an Sc template for the late-type systems. No correction was made for galaxies classified as unknown. This k-correction generally amounts to only a tenth or few tenths correction to the magnitudes, with larger values for more distant galaxies ($z > 0.2$). Finally, we converted the k-corrected, apparent R-band magnitudes into luminosities relative to L^* with the luminosity distance calculated using the assumed WMAP cosmology.

In total, we obtained spectra for 2933 sources and confirmed 2800 redshifts. Of these, there are 1198 galaxies with $0.005 < z < (z_{\rm em} - 0.01)$ which are suitable for studying the association between galaxies and absorption lines in the low-z IGM. The properties of these galaxies are summarized in Table 4. Lastly, Table 1 lists the spectroscopic completeness of each field as a function of magnitude limit and angular offset from the quasar, e.g. $C^{5'}_{19.5}$ gives the completeness percentile to $R = 19.5$ mag and $\theta_{\rm max} = 5'$ offset from the quasar.

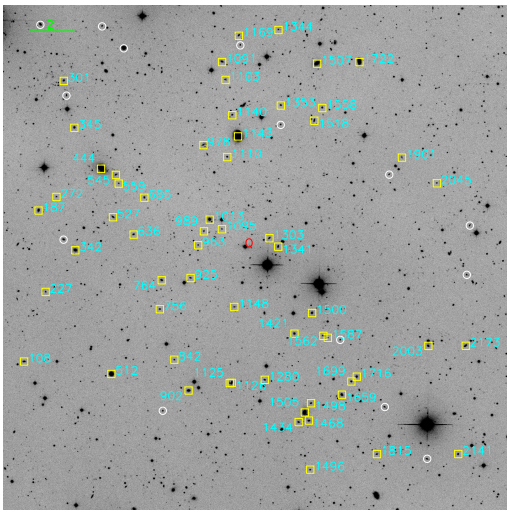


FIG. 2.— R-band image of the field surrounding Q0026+1259 ($z_{\rm em} = 0.142$; marked with a red "Q"). All galaxies with $z < (z_{\rm em} + 0.01)$ are labelled with their redshifts. Unless otherwise indicated, labels are placed to the right and just above the galaxy. Objects circled in pink were targeted (i.e. $R < 19.5$ mag and the imaging indicated it was not a point source) but no redshift was determined either because no mask included it or a secure redshift could not be determined from the spectrum.

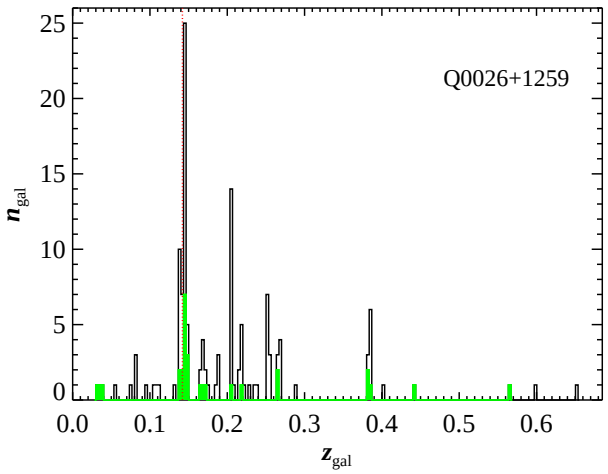


FIG. 3.— Histogram of galaxy redshifts for the field surrounding Q0026+1259 ($z_{\rm em} = 0.142$), binned in intervals of $\Delta z = 0.00333$. The solid (green) histogram shows the distribution for galaxies within $5'$ of the quasar while the open (black) histogram is for all galaxies surveyed in the field. The dotted (red) vertical line indicates the quasar emission-line redshift ($z_{\rm em}$).

3.1. *Q0026+1259*

To date this quasar has no published list of IGM absorption lines, presumably because its UV spectroscopic dataset is relatively sparse. Figure 2 shows the field and marks the galaxies surrounding the quasar with measured redshifts. Figure 3 shows a histogram of the redshifts of the galaxies in the field surrounding the quasar.

TABLE 4
SUMMARY OF GALAXIES AT $z < z_{\rm em} + 0.01$

ID	RA (J2000)	DEC (J2000)	$z_{\rm gal}$	L^a ($L*$)	ρ^b (h_{72}^{-1} kpc)	Type^c
Q0026+1259: $0.005 < z < (z_{\rm em} - 0.01)$						
Q0026+1259_1303	00:29:09.2	+13:16:28	0.03295	0.02	44	Late
Q0026+1259_1500	00:29:01.3	+13:13:12	0.03346	0.03	158	Late
Q0026+1259_1143	00:29:15.3	+13:20:57	0.03931	1.38	214	Early
Q0026+1259_1140	00:29:16.4	+13:21:52	0.08043	0.11	497	Unkn
Q0026+1259_1722	00:28:53.5	+13:24:19	0.05645	0.56	595	Late
Q0026+1259_1103	00:29:17.7	+13:23:26	0.08073	0.08	634	Unkn
Q0026+1259_1901	00:28:45.5	+13:20:08	0.08062	0.06	695	Early
Q0026+1259_902	00:29:23.4	+13:09:41	0.11253	1.09	781	Late
Q0026+1259_1125	00:29:16.0	+13:10:03	0.13138	0.18	791	Unkn
Q0026+1259_512	00:29:37.5	+13:10:21	0.09614	1.96	821	Early
Q0026+1259_108	00:29:53.3	+13:10:50	0.07379	0.19	879	Early
Q0026+1259_2045	00:28:39.0	+13:19:02	0.10711	0.14	1007	Early
Q0026+1259_2141	00:28:34.3	+13:07:05	0.10499	0.36	1437	Early
Q0026+1259: $(z_{\rm em} - 0.01) < z < (z_{\rm em} + 0.01)$						
Q0026+1259_1095	00:29:17.9	+13:16:50	0.14736	0.20	186	Early
Q0026+1259_1341	00:29:07.6	+13:16:06	0.14599	0.95	219	Early
Q0026+1259_989	00:29:21.2	+13:16:44	0.14802	0.27	285	Late
Q0026+1259_1013	00:29:20.2	+13:17:15	0.14651	2.79	286	Early
Q0026+1259_963	00:29:22.2	+13:16:06	0.14183	0.21	294	Early
Q0026+1259_1148	00:29:15.4	+13:13:25	0.14487	0.17	381	Late
Q0026+1259_925	00:29:23.4	+13:14:39	0.14480	0.29	398	Late
Q0026+1259_764	00:29:28.7	+13:14:32	0.14553	1.06	575	Late
Q0026+1259_1110	00:29:17.2	+13:20:01	0.14655	0.49	582	Late
Q0026+1259_1421	00:29:04.4	+13:12:17	0.14009	0.95	614	Early

NOTE. — [The complete version of this table is in the electronic edition of the Journal. The printed edition contains only a sample.]

[a] Luminosity relative to L* as measured from the apparent R-band magnitude. See text for a detailed description.

[b] Impact parameter in physical distance.

[c] The galaxy type is a crude assessment of the spectrum based on a fit of eigenfunctions. See text for a detailed description.

TABLE 5
Q0026+1259: OBJECT SUMMARY

ID	RA	DEC	B (mag)	R (mag)	S/G^a	Area ($\Box''$)	flg^b	z
1	00:28:40.3	+13:08:22	11.51 ± 0.11	10.20 ± 0.08	0.69	76.8	0	···
2	00:28:27.4	+13:16:27	18.79 ± 0.12	17.43 ± 0.08	0.96	4.8	0	···
3	00:28:27.6	+13:26:27	19.12 ± 0.12	17.33 ± 0.08	1.00	2.6	0	···
4	00:28:26.8	+13:15:39	19.54 ± 0.12	18.21 ± 0.08	1.00	2.4	0	···
5	00:28:27.2	+13:24:49	20.46 ± 0.14	18.22 ± 0.08	1.00	2.4	0	···
6	00:28:26.4	+13:14:06	21.46 ± 0.23	19.60 ± 0.09	0.14	3.6	0	···
7	00:28:26.1	+13:13:18	21.76 ± 0.27	19.50 ± 0.09	1.00	2.9	0	···
8	00:28:25.8	+13:10:15	23.74 ± 1.00	21.42 ± 0.15	0.19	2.4	0	···
9	00:28:25.8	+13:10:33	21.64 ± 0.24	19.64 ± 0.09	0.87	2.6	0	···
10	00:28:25.9	+13:11:33	20.69 ± 0.16	18.26 ± 0.08	1.00	2.4	0	···

NOTE. — [The complete version of this table is in the electronic edition of the Journal. The printed edition contains only a sample.]

[a] Star/galaxy classifier calculated by SExtractor. Values near unity indicate a stellar-like point-spread function.

[b] This binary flag has the following code: 1: Survey target; 2: Spectrum taken; 4: Redshift measured.

There is a relatively large 'spike' at the quasar redshift ($z_{\rm em} = 0.142$) which marks a galaxy group (several $L \approx L*$ galaxies lie within $\rho = 300\,$kpc). One identifies no other significant large-scale structures foreground to the quasar in our LCO/WFCCD survey. Table 5 summarizes the photometry and spectroscopy for galaxies and stars in the field surrounding Q0026+1259.

3.2. *Ton S 180*

The Ton S 180 sightline has been surveyed for Lyα absorption by (Penton et al. 2004, STIS/G140M spectra) and for O VI absorption by (Danforth et al. 2006, *FUSE)*. The latter report O VI absorbers at $z = 0.0234, 0.0436$ and $z = 0.0456$, each of which shows a galaxy within an impact parameter of $\rho < 300\,$kpc and within a velocity offset of $|\delta v| < 300$km s^{-1}. None of these were reported in Stocke et al. (2006)[10] presumably because these galaxies were fainter than the magnitude limit of their galaxy compilation. Wakker & Savage (2009) also associated galaxies at $z \approx 0$ with Lyα and O VI absorption along this sightline.

Figure 4 shows the field and marks the galaxies surrounding the quasar with measured redshifts. Given the low emission redshift of the quasar, there are only a handful of galaxies identified in its foreground. One also notes several bright galaxies coincident with the quasar redshift and at relatively small impact parameter ($\rho \approx 300\,$kpc). Figure 5 shows a histogram of the redshifts of the galaxies in the field surrounding the quasar. Table 6 summarizes the photometry and spectroscopy of our survey for galaxies and stars in the field surrounding Ton S 180.

3.3. *Ton S 210*

Although the quasar Ton S 210 has an impressive UV spectroscopic dataset, there is no published survey for IGM absorption beyond the very local universe (Wakker & Savage 2009). Coincidentally, we have discovered very few galaxies foreground to the quasar to our magnitude limit (Figure 6, Table 4) despite obtaining spectra for 71 extragalactic sources (Figure 7, Table 7). None of the foreground sources lie at close impact parameter.

3.4. *PKS0312−770*

We previously published the spectrum of a galaxy associated with the $z \approx 0.21$ Lyman limit system toward PKS0312−770 (Lehner et al. 2009). The sightline has also been surveyed by several groups for Lyα and O VI absorption (Danforth & Shull 2008; Thom & Chen 2008; Tripp et al. 2008). Tripp et al. (2008) report two O VI absorbers at $z = 0.1589$ and $z = 0.19827$ where we identify bright galaxies in our survey but only at large impact parameters ($\rho > 500\,$kpc). We also identify a galaxy at $z = 0.0736$ with $\rho = 954\,$kpc that may be associated with the 'void' absorber reported by Stocke et al. (2006). It has a luminosity $L \approx 0.1L*$ which places it below their survey limit.

Tables 8 summarizes the photometry and spectroscopy for galaxies and stars in the field surrounding PKS0312–770. Figure 8 displays our imaging data which covers a rectangular $15' \times 32'$ field of view, and Figure 9 shows a redshift histogram for the field.

[10] Indeed, they remarked that the O VI absorber at $z = 0.436$ was the "most isolated" of their sample with no bright galaxy within 1 Mpc.

3.5. *PKS0405–123*

This field has received significant attention over the past decade, largely because of its relatively high redshift but also because it exhibits several strong O VI absorbers (Chen & Prochaska 2000; Prochaska et al. 2004; Chen et al. 2005; Prochaska et al. 2006; Williger et al. 2006; Tripp et al. 2008; Howk et al. 2009; Wakker & Savage 2009; Savage et al. 2010). We published the results of our galaxy survey in Chen et al. (2005) and Prochaska et al. (2006); here we only summarize properties of the galaxies close to the sightline (Table 4). We also remind the reader that our galaxy survey had non-uniform spectral and imaging coverage beyond the inner $\approx 20' \times 20'$ field-of-view.

3.6. *PKS0558–504*

This quasar has a very limited UV spectral dataset, and the only IGM analysis has been performed at $z \approx 0$ (Wakker & Savage 2009). By chance, our survey also shows no galaxies at low impact parameters (Tables 9 and Table 4). Figure 10 shows the field and marks the galaxies surrounding the quasar with measured redshifts and Figure 11 presents a redshift histogram.

3.7. *PG1004+130*

This sightline has been analyzed for Lyα absorption by Bowen et al. (2002) who associated a cluster of low z Lyα absorption lines with a bright nearby galaxy (UGC 5454). A relatively high quality *FUSE* dataset exists but has not yet been surveyed for O VI absorption. As discussed in Prochaska et al. (in prep), we have also analyzed these UV datasets for Lyα and O VI absorption at the redshifts of the galaxies in our LCO/WFCCD survey with small impact parameter to the sightline (Table 4).

The photometry and spectroscopy of our full survey is listed in Table 10 and Figure 12 shows the field and marks the galaxies surrounding the quasars with determined redshifts. Figure 13 provides a redshift histogram.

3.8. *HE1029-140*

This quasar has a modest UV spectral dataset and has been analyzed for Lyα absorption by Penton et al. (2004). Figure 14 shows the field and marks the few galaxies with $z < z_{\rm em}$ that we have identified in the LCO/WFCCD survey. Table 11 summarizes the photometry and spectroscopy of all objects in the field and Figure 15 gives a redshift histogram of the galaxies from our survey.

3.9. *PG1116+215*

This sightline has been studied by Tripp et al. (1998) and Sembach et al. (2004) for absorption lines and associated galaxies, along with several other more recent analyses (Tripp et al. 2008; Danforth & Shull 2008; Wakker & Savage 2009). They identify three O VI systems foreground to the quasar at $z = 0.0597, 0.13879$ and 0.1655. Each of these is associated with a galaxy at $\rho \leq 150\,$kpc in our survey. For the $z = 0.0597$ system, we identify 6 galaxies within 1 Mpc including several with

$L \gtrsim L^*$ which suggests a group environment (Table 4). None of these galaxies were identified in previous surveys.

Table 12 summarizes the photometry and spectroscopy for the objects that we surveyed in the field surrounding PG1116+215. Figure 16 presents an image of the field and marks the galaxies surrounding the quasar with determined $z < z_{\rm em}$ and Figure 17 shows a redshift histogram of the full galaxy survey.

3.10. *PG1211+143*

Tumlinson et al. (2005) analyzed this field for IGM absorption lines and corresponding galaxies. They reported a pair of O VI systems at $z = 0.0513$ and 0.0645 and associated these with $L \approx L*$ galaxies at $\rho \approx 150$ kpc. Our survey includes these two galaxies (Table 4) and an additional, fainter galaxy at significantly smaller impact parameter for the system at $z = 0.0646$ ($\rho = 70$ kpc). We also identify additional galaxies associated with the galaxy group at $z = 0.0513$. Wakker & Savage (2009) also analyzed this field, focusing on $z \approx 0$.

Table 13 summarizes the photometry and spectroscopy for galaxies and stars in the field surrounding PG1211+143. Figure 18 shows the field and marks the galaxies surrounding the quasar while Figure 19 gives a galaxy redshift histogram.

3.11. *PG1216+069*

This sightline has been studied for absorption by multiple groups (Tripp et al. 2008; Thom & Chen 2008; Danforth & Shull 2008; Chen & Mulchaey 2009; Wakker & Savage 2009) with O VI systems reported at $z = 0.1236, 0.268$ and 0.282. Our survey reveals galaxies at every redshift, but only the lowest redshift system shows an example with small impact parameter ($\rho = 85$ kpc). In addition, we report an overdensity of galaxies at $z = 0.0805$ (5 galaxies within 1 Mpc including an L^* galaxy; Table 4) which is associated with strong Lyα absorption but no apparent O VI gas to a sensitive limit.

The sightline is also notable for intersecting Virgo, and Tripp et al. (2005) report on a strong H I absorber near the NGC 4261 group ($z = 0.0063$). No apparent O VI absorption is detected at the redshift of either structure although the equivalent width limits are poor from the *FUSE* spectra at these wavelengths.

Table 14 summarizes the photometry and spectroscopy, Figure 20 shows the field and marks the galaxies surrounding the quasars with determined redshifts. Figure 21 shows a histogram of the redshifts of the galaxies in the field surrounding the quasar.

3.12. *3C273*

Because of its very high UV flux, this quasar and the field around it have been the subject of many previous studies including some of the first galaxy surveys along quasar sightlines (Morris et al. 1993). Tripp et al. (2008) report O VI detections at several redshifts, all at column densities that lie below the sensitivity limit of most other UV spectral datasets, i.e. $N(O^{+5}) < 10^{13.5}\,{\rm cm}^{-2}$. None of these absorbers shows a corresponding galaxy in our survey with $\rho < 300$ kpc, but we do identify galaxies at larger impact parameter (Table 4). Wakker & Savage (2009) also analyzed this field, focusing on $z \approx 0$.

Table 15 summarizes the photometry and spectroscopy for galaxies and stars in the field surrounding 3C273. Figure 22 shows the field and marks the galaxies surrounding the quasars with determined redshifts. Figure 23 shows a histogram of the redshifts of the galaxies in the field surrounding the quasar.

3.13. *Q1230+095*

This quasar has a very sparse UV spectral dataset and there is no published list of IGM absorption. We emphasize that the quasar's redshift ($z_{\rm em} = 0.415$) make it a very promising sightline for studying the IGM/galaxy connection. Furthermore, there is a set of galaxies at small impact parameters revealed by our survey (Figure 24, Table 4). We encourage observations with the *HST*/COS instrument. Table 16 summarizes the full photometry and spectroscopy for objects in the field surrounding Q1230+095 and Figure 25 histograms the galaxy redshifts.

3.14. *PKS1302-102*

This field has been surveyed for Lyα and O VI absorption by several groups (Danforth et al. 2006; Cooksey et al. 2008; Danforth & Shull 2008; Thom & Chen 2008; Tripp et al. 2008; Wakker & Savage 2009). These groups have reported O VI detections at multiple redshifts: $z = 0.0423, 0.0647, 0.0940, 0.0989, 0.1453, 0.1916, 0.2256$, and 0.2274. Our survey has revealed nearly 100 galaxies foreground to the quasar including several at impact parameters $\rho < 100$ kpc (see also Cooksey et al. 2008). We detect galaxy within 300 kpc and with $|\delta v| < 400$km s^{-1} for each absorber at $z < 0.2$ except at $z = 0.0989$. This includes two sub-$L*$ galaxies that lie at low impact parameter ($\rho < 100$ kpc; Table 4, Figure 26). Table 17 summarizes the photometry and spectroscopy for galaxies and stars in the field and Figure 27 presents a redshift histogram of all galaxies.

3.15. *PG1307+085*

This quasar has only a sparse dataset of UV spectroscopy and there is no published list for Lyα or O VI absorption systems. Its relatively high redshift ($z_{\rm em} = 0.155$) marks it as a valuable sightline for future study and our survey provides a modest set of galaxies for cross-correlation analysis (Table 4). The full photometry and spectroscopy for objects from our survey in the field are listed in Table 18. Figure 28 presents an R-band image of the field and marks the surrounding galaxies with $z < z_{\rm em}$. Figure 29 shows a redshift histogram for the galaxies we have discovered.

3.16. *MRK1383*

Despite its low redshift and correspondingly small pathlength, this sightline has been studied extensively for Lyα and O VI absorption (Danforth et al. 2006; Danforth & Shull 2008; Wakker & Savage 2009). Our survey reveals only a handful of galaxies with $z < z_{\rm em}$ (Table 4, Figure 30), but we also note that this field has one of the lowest completeness levels to $R = 19.5$ mag (80%). Table 19 summarizes the photometry and spectroscopy for galaxies and stars in the field surrounding MRK1383. Figure 30 provides an image of the field and

marks the foreground galaxies, and Figure 31 shows a redshift histogram for the galaxies.

3.17. *Q1553+113*

This quasar boasts only a short *FUSE* exposure and no additional UV spectroscopy. It has been surveyed for IGM absorption only at $z \approx 0$ by Wakker & Savage (2009). Given the extensive dataset of galaxies that we have discovered in the foreground (Table 4, Figure 32), we encourage future observations with *HST*/COS. The photometry and spectroscopy for objects from our survey in the field are listed in Table 20 and a redshift histogram for the galaxies is provided by Figure 33.

3.18. *PKS2005-489*

This sightline has been surveyed for Lyα and O VI absorption over the relatively short pathlength provided by this $z = 0.071$ AGN (Penton et al. 2004; Danforth et al. 2006; Danforth & Shull 2008). There are no O VI systems reported. Our survey reveals two sets of foreground galaxies at redshifts $z \approx 0.045$ and 0.057, but none at very close impact parameter to the sightline (Figure 34, Table 4). Table 21 summarizes the photometry and spectroscopy for all objects in the field surrounding PKS2005–489. Figure 35 presents a redshift histogram for all of the galaxies in our survey.

3.19. *FJ2155-092*

The quasar FJ2155–092, also known as PHL 1811, has a high quality UV spectral dataset. Jenkins et al. (2005) has published an analysis of the Lyman limit system at $z = 0.081$ and its neighboring galaxies. Other groups have examined the spectra for Lyα and O VI absorption (Tripp et al. 2008; Danforth & Shull 2008; Wakker & Savage 2009). Altogether, the sightline boasts four O VI systems at $z = 0.0788, 0.1326, 0.1581$ and 0.1769, all of which have a neighboring galaxy in our survey with $\rho < 350\,\mathrm{kpc}$ and $|\delta v| < 400\mathrm{km\ s^{-1}}$ but none at very low impact parameter. Figure 36 shows the field and marks the galaxies foreground to the quasar with determined redshifts. Table 22 lists the photometry and spectroscopy for galaxies and stars throughout the field and a redshift histogram of the galaxies is given by Figure 37.

3.20. *PKS2155-304*

This sightline has received significant attention, primarily because of the claimed (and debated) O VII and O VIII absorption at $z \approx 0.055$ (Fang et al. 2002; Cagnoni et al. 2003). The high quality UV spectral datasets have also been surveyed for Lyα and O VI absorption (who report detections at $z = 0.0541$ and 0.0571 Danforth et al. 2006; Danforth & Shull 2008; Wakker & Savage 2009). We associate each of these with a bright ($L > L*$) galaxy in our survey but at relatively large impact parameter ($\rho \sim 500\,\mathrm{kpc}$). The photometry and spectroscopy for our survey of the the field is given in Table 23. We show an image of the field and mark the foreground galaxies in Figure 38 and present a redshift histogram for all of the galaxies in Figure 39. We note that our deeper survey reveals no additional galaxies at $z \approx 0.055$ from the ones first reported by (see Table 4; Shull et al. 2003).

FIG. 4.— Same as for Figure 2 but for the field surrounding Ton S 180 ($z_{\rm em} = 0.062$).

FIG. 5.— Same as for Figure 3 but for the field surrounding Ton S 180 ($z_{\rm em} = 0.062$).

FIG. 6.— Same as for Figure 2 but for the field surrounding Ton S 210 ($z_{\rm em} = 0.116$).

FIG. 7.— Same as for Figure 3 but for the field surrounding Ton S 210 ($z_{\rm em} = 0.116$).

FIG. 8.— Same as for Figure 2 but for the field surrounding PKS0312–770 ($z_{\rm em} = 0.223$).

FIG. 9.— Same as for Figure 3 but for the field surrounding PKS0312–770 ($z_{\rm em} = 0.223$).

FIG. 10.— Same as for Figure 2 but for the field surrounding PKS0558–504 ($z_{\rm em} = 0.137$).

FIG. 11.— Same as for Figure 3 but for the field surrounding PKS0558–504 ($z_{\rm em} = 0.137$).

FIG. 12.— Same as for Figure 2 but for the field surrounding PG1004+130 ($z_{\rm em} = 0.240$).

FIG. 13.— Same as for Figure 3 but for the field surrounding PG1004+130 ($z_{\rm em} = 0.240$).

FIG. 14.— Same as for Figure 2 but for the field surrounding HE1029–140 ($z_{\rm em} = 0.086$).

FIG. 15.— Same as for Figure 3 but for the field surrounding HE1029–140 ($z_{\rm em} = 0.086$).

FIG. 16.— Same as for Figure 2 but for the field surrounding PG1116+215 ($z_{\rm em} = 0.177$).

FIG. 17.— Same as for Figure 3 but for the field surrounding PG1116+215 ($z_{\rm em} = 0.177$).

FIG. 18.— Same as for Figure 2 but for the field surrounding PG1211+143 ($z_{\rm em} = 0.809$).

FIG. 19.— Same as for Figure 3 but for the field surrounding PG1211+143 ($z_{\rm em} = 0.809$).

FIG. 20.— Same as for Figure 2 but for the field surrounding PG1216+069 ($z_{\rm em} = 0.331$).

FIG. 21.— Same as for Figure 3 but for the field surrounding PG1216+069 ($z_{\rm em} = 0.331$).

FIG. 22.— Same as for Figure 2 but for the field surrounding 3C273 ($z_{\rm em} = 0.158$).

FIG. 23.— Same as for Figure 3 but for the field surrounding 3C273 ($z_{\rm em} = 0.158$).

FIG. 24.— Same as for Figure 2 but for the field surrounding Q1230+095 ($z_{\rm em} = 0.415$).

FIG. 25.— Same as for Figure 3 but for the field surrounding Q1230+095 ($z_{\rm em} = 0.415$).

FIG. 26.— Same as for Figure 2 but for the field surrounding PKS1302–102 ($z_{\rm em} = 0.286$).

FIG. 27.— Same as for Figure 3 but for the field surrounding PKS1302–102 ($z_{\rm em} = 0.286$).

FIG. 28.— Same as for Figure 2 but for the field surrounding PG1307+085 ($z_{\rm em} = 0.155$).

FIG. 29.— Same as for Figure 3 but for the field surrounding PG1307+085 ($z_{\rm em} = 0.155$).

FIG. 30.— Same as for Figure 2 but for the field surrounding MRK1383 ($z_{\rm em} = 0.086$).

FIG. 31.— Same as for Figure 3 but for the field surrounding MRK1383 ($z_{\rm em} = 0.086$).

FIG. 32.— Same as for Figure 2 but for the field surrounding Q1553+113 ($z_{\rm em} = 0.360$).

FIG. 33.— Same as for Figure 3 but for the field surrounding Q1553+113 ($z_{\rm em} = 0.360$).

FIG. 34.— Same as for Figure 2 but for the field surrounding PKS2005–489 ($z_{\rm em} = 0.071$).

FIG. 35.— Same as for Figure 3 but for the field surrounding PKS2005–489 ($z_{\rm em} = 0.071$).

FIG. 36.— Same as for Figure 2 but for the field surrounding FJ2155–092 ($z_{\rm em} = 0.170$).

FIG. 37.— Same as for Figure 3 but for the field surrounding FJ2155–092 ($z_{\rm em} = 0.170$).

FIG. 38.— Same as for Figure 2 but for the field surrounding PKS2155–304 ($z_{\rm em} = 0.116$).

FIG. 39.— Same as for Figure 3 but for the field surrounding PKS2155–304 ($z_{\rm em} = 0.116$).

4. SUMMARY

This paper serves to define our LCO/WFCCD galaxy survey which was designed to study the IGM/galaxy connection at $z \lesssim 0.2$. We have listed R-band photometry for objects in each field, identified the objects which satisfy our targeting criteria, provide (online) the extracted and coadded 1D spectra, and tabulate the redshifts for all sources with an unambiguous identification. Table 4 summarizes properties of the galaxies discovered in the 20 fields restricted to $0.005 < z < (z_{\rm em} + 0.01)$. Again, we note that approximately half of the fields have been surveyed for galaxies by other groups that our results should not be considered a complete census. This table and the redshift histograms reveal the types of galaxy overdensities that are typical of other low z galaxy surveys.

Figure 40 presents a color-magnitude diagram for the galaxies, and summarizes the redshift, luminosity, and impact parameter distributions of the sample. The set of galaxies with $z < (z_{\rm em} - 0.01)$ is predominantly at redshifts $z = 0.1 - 0.3$, with luminosities $L = 0.1$–$5L^*$, and located at impact parameters of several hundred kpc from the quasar. These distributions are a complex convolution of the magnitude limit and angular extent of the survey fields, and the emission redshift distribution of the targeted quasars. For example, the impact parameter distribution does not scale as $N \propto \rho$ because the fixed angular extent of the survey restricts galaxies to $\rho < 1\,{\rm Mpc}$ at $z < 0.1$. Nevertheless, Figure 40 provides an overview of this survey's utility for probing the low z IGM.

To crudely assess the completeness and global characteristics of the survey, we have also constructed an R-band luminosity function from the dataset. Specifically, we restricted the survey of each field to $R_{\rm max} = 19.5\,{\rm mag}$, $\theta_{\rm max} = 10'$, and $0.02 < z < min[(z_{\rm em} - 0.01), 0.2]$. The maximum redshift was imposed to minimize effects from having targeted fields with a known, luminous quasar and also to facilitate comparison with the Sloan Digital Sky Survey (SDSS). We calculated the effective comoving volume $V_{\rm eff}$ for a given absolute magnitude M and evaluated the luminosity function,

$$\Phi(M) = \frac{n_{\rm gal}}{V_{\rm eff}\,\Delta M} \quad , \qquad (1)$$

within magnitude bins of $\Delta M = 0.5\,{\rm mag}$. The analysis was further restricted to the 17 fields which have a completeness percentile $C^{10'}_{19.5} > 70\%$ (Table 1). The raw evaluation of $\Phi(M)$ is shown as black points in the lower panel of Figure 41, where the error bars reflect only Poisson uncertainty (1σ equivalent) in $n_{\rm gal}$. Upper limits correspond to 95% c.l. We have also performed a jackknife analysis of the survey and recover similar scatter in the measurements albeit with a bias toward lower values.

We have also attempted to correct for incompleteness in the survey, using two approaches. The blue stars in the figure include a completeness correction estimated by scaling $n_{\rm gal}$ in each field by its corresponding completeness, i.e. $1/C^{10'}_{19.5}$. This increases $\Phi(M)$ in nearly every bin by $\approx 20\%$, i.e. the correction is essentially independent of apparent magnitude. As Figure 42 demonstrates, however, the survey has higher incompleteness for fainter galaxies. Therefore, we have used the results given in Figure 42 to increment the contribution of each galaxy to $\Phi(M)$ according to each galaxy's apparent magnitude. These results are shown as the cyan diamonds in Figure 41.

Overplotted on our evaluations of $\Phi(M)$ are the luminosity functions derived for the r-band from the Sloan Digital Sky Survey (Blanton et al. 2003; Montero-Dorta & Prada 2009), transformed to our assumed cosmology (e.g. $h = 0.72$). The agreement between our evaluation and the SDSS estimations is remarkably good. The only significant deviation is at the bright-end where we have detected 2–3× more galaxies than predicted by the SDSS luminosity functions. The offset could be the result of an Eddington bias in our estimation of $\Phi(M)$ and/or a modest offset between our R-band photometry and the SDSS r-band (there is one notable for some of these galaxies which are also observed by SDSS). We also emphasize that the number of galaxies in these deviant bins is small (~ 20; upper panel of Figure 41). We conclude, therefore, that our combined survey provides a reasonably representative sample of galaxies for low-z IGM analysis.

In future papers (e.g. Prochaska et al. 2011, in prep), we explore the association of galaxies and their structures to the IGM with particular focus on H I Lyα and O VI absorption. We also encourage the acquisition of new, more sensitive UV spectral datasets (i.e. with *HST*/COS) to further enhance this galaxy survey.

J. X. P. is partially supported by an NSF CAREER grant (AST–0548180). We recognize the terrific staff at Las Campanas Observatory who were instrumental in carrying out this program. We kindly thank R. Weymann who built the WFCCD spectrograph and supported this program.

REFERENCES

Barton, E. J., & Cooke, J. 2009, AJ, 138, 1817
Bergeron, J., & Boisse, P. 1991, Advances in Space Research, 11, 241
Bertin, E., & Arnouts, S. 1996, Astronomy and Astrophysics Supplement, 117, 393
Blanton, M. R., et al. 2003, ApJ, 594, 186
Bowen, D. V., Jimenez, R., Jenkins, E. B., & Pettini, M. 2001, ApJ, 547, 39
Bowen, D. V., Pettini, M., & Blades, J. C. 2002, ApJ, 580, 169
Cagnoni, I., Nicastro, F., Maraschi, L., Treves, A., & Tavecchio, F. 2003, New A Rev., 47, 561
Cen, R., & Ostriker, J. P. 1999, ApJ, 514, 1
Chen, H., Helsby, J. E., Gauthier, J., Shectman, S. A., Thompson, I. B., & Tinker, J. L. 2010, ApJ, 714, 1521
Chen, H., & Mulchaey, J. S. 2009, ApJ, 701, 1219
Chen, H.-W., & Prochaska, J. X. 2000, ApJ, 543, L9
Chen, H.-W., Prochaska, J. X., Weiner, B. J., Mulchaey, J. S., & Williger, G. M. 2005, ApJ, 629, L25
Cooksey, K. L., Prochaska, J. X., Chen, H.-W., Mulchaey, J. S., & Weiner, B. J. 2008, ApJ, 676, 262
Danforth, C. W., & Shull, J. M. 2008, ApJ, 679, 194
Danforth, C. W., Shull, J. M., Rosenberg, J. L., & Stocke, J. T. 2006, ApJ, 640, 716
Davé, R., et al. 2001, ApJ, 552, 473
Dunkley, J., et al. 2009, ApJS, 180, 306
Fang, T., & Bryan, G. L. 2001, ApJ, 561, L31
Fang, T., Marshall, H. L., Lee, J. C., Davis, D. S., & Canizares, C. R. 2002, ApJ, 572, L127

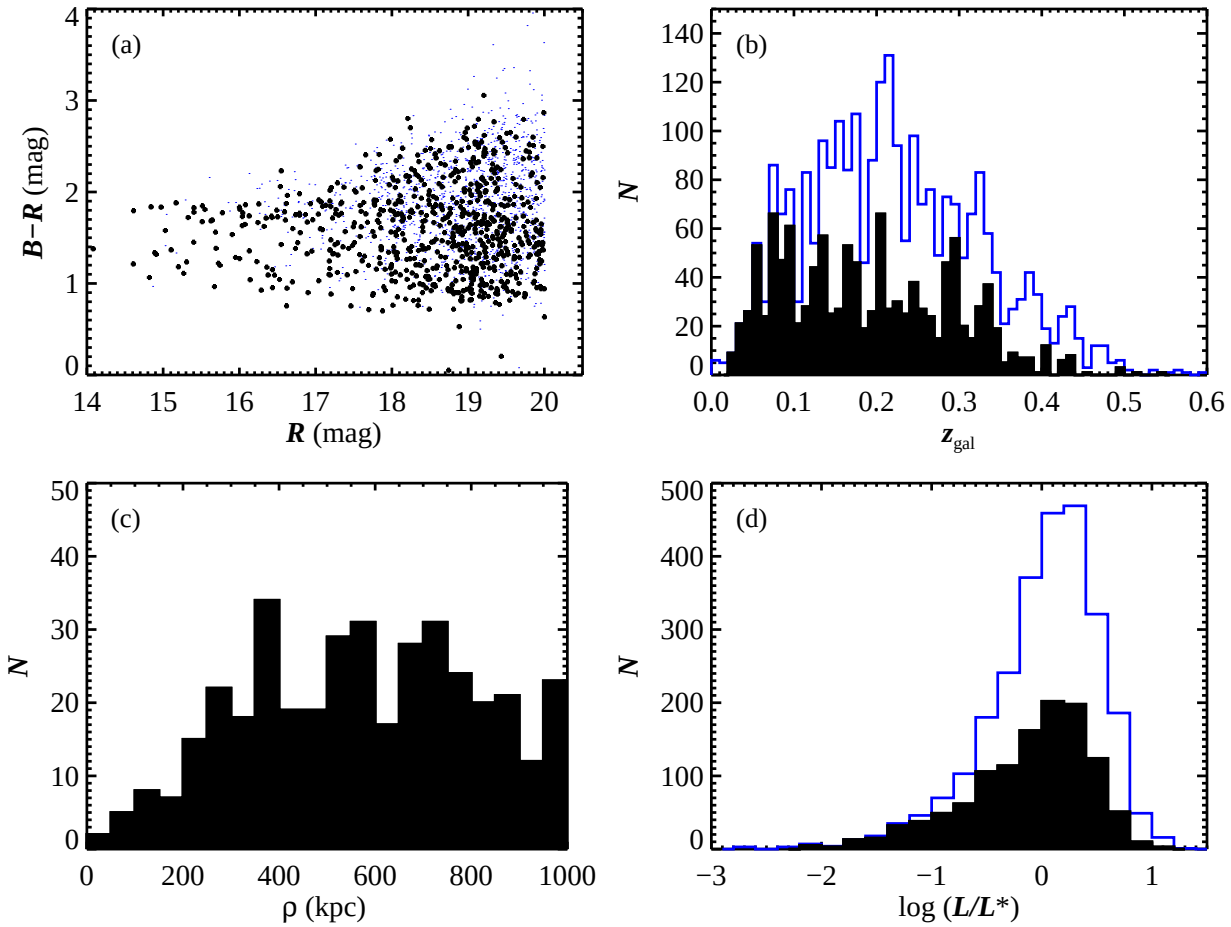


FIG. 40.— (a) Color-magnitude diagram of all galaxies with redshifts $z > 0.005$ (blue dots) in LCO/WFCCD survey and galaxies with $0.02 < z < (z_{\rm em} - 0.01)$ (black symbols). (b) Histogram of the galaxy redshifts for sources detected in our survey. The open (blue) histogram shows all sources with $z > 0.005$, while the solid black histogram is restricted to $0.02 < z < (z_{\rm em} - 0.01)$ and therefore represents the sample that may be used to study associations with the low z IGM. (c) Distribution of impact parameters ρ for the galaxies in our survey with $0.02 < z < (z_{\rm em} - 0.01)$. The incidence of objects does not increase as $N \propto \rho$ for $\rho \gtrsim 400$ kpc because of the (nearly) fixed angular extent of the survey. (d) Luminosity distribution for the galaxies in our LCO/WFCCD survey restricted to the sample of sources with $z > 0.005$ (blue, open histogram) and $0.02 < z < (z_{\rm em} - 0.01)$ (black, solid histogram).

Howk, J. C., Ribaudo, J. S., Lehner, N., Prochaska, J. X., & Chen, H. 2009, MNRAS, 396, 1875
Jenkins, E. B., Bowen, D. V., Tripp, T. M., & Sembach, K. R. 2005, ApJ, 623, 767
Landolt, A. U. 1992, AJ, 104, 372
Lanzetta, K. M., Bowen, D. V., Tytler, D., & Webb, J. K. 1995, ApJ, 442, 538
Lehner, N., Prochaska, J. X., Kobulnicky, H. A., Cooksey, K. L., Howk, J. C., Williger, G. M., & Cales, S. L. 2009, ApJ, 694, 734
Montero-Dorta, A. D., & Prada, F. 2009, MNRAS, 399, 1106
Morris, S. L., Weymann, R. J., Dressler, A., McCarthy, P. J., Smith, B. A., Terrile, R. J., Giovanelli, R., & Irwin, M. 1993, ApJ, 419, 524
Oppenheimer, B. D., & Davé, R. 2009, MNRAS, 395, 1875
Penton, S. V., Stocke, J. T., & Shull, J. M. 2004, ApJS, 152, 29
Prochaska, J. X., Chen, H.-W., Howk, J. C., Weiner, B. J., & Mulchaey, J. 2004, ApJ, 617, 718
Prochaska, J. X., Weiner, B. J., Chen, H.-W., & Mulchaey, J. S. 2006, ApJ, 643, 680
Savage, B. D., et al. 2010, ApJ, 719, 1526
Savage, B. D., Sembach, K. R., Tripp, T. M., & Richter, P. 2002, ApJ, 564, 631
Scannapieco, E., Pichon, C., Aracil, B., Petitjean, P., Thacker, R. J., Pogosyan, D., Bergeron, J., & Couchman, H. M. P. 2006, MNRAS, 365, 615
Sembach, K. R., Tripp, T. M., Savage, B. D., & Richter, P. 2004, ApJS, 155, 351
Shone, A. M., Morris, S. L., Crighton, N., & Wilman, R. J. 2010, MNRAS, 402, 2520
Shull, J. M., Stocke, J. T., & Penton, S. 1996, AJ, 111, 72
Shull, J. M., Tumlinson, J., & Giroux, M. L. 2003, ApJ, 594, L107
Steidel, C. C. 1993, in Astrophysics and Space Science Library, Vol. 188, The Environment and Evolution of Galaxies, ed. J. M. Shull & H. A. Thronson, 263–+
Stocke, J. T., Penton, S. V., Danforth, C. W., Shull, J. M., Tumlinson, J., & McLin, K. M. 2006, ApJ, 641, 217
Stocke, J. T., Shull, J. M., Penton, S., Donahue, M., & Carilli, C. 1995, ApJ, 451, 24
Stoughton, C., et al. 2002, AJ, 123, 485
Thom, C., & Chen, H. 2008, ApJ, 683, 22
Tripp, T. M., Aracil, B., Bowen, D. V., & Jenkins, E. B. 2006, ApJ, 643, L77
Tripp, T. M., Jenkins, E. B., Bowen, D. V., Prochaska, J. X., Aracil, B., & Ganguly, R. 2005, ApJ, 619, 714
Tripp, T. M., Lu, L., & Savage, B. D. 1998, ApJ, 508, 200
Tripp, T. M., & Savage, B. D. 2000, ApJ, 542, 42
Tripp, T. M., Sembach, K. R., Bowen, D. V., Savage, B. D., Jenkins, E. B., Lehner, N., & Richter, P. 2008, ApJS, 177, 39
Tumlinson, J., Shull, J. M., Giroux, M. L., & Stocke, J. T. 2005, ApJ, 620, 95
Wakker, B. P., & Savage, B. D. 2009, ApJS, 182, 378
Wiersma, R. P. C., Schaye, J., Dalla Vecchia, C., Booth, C. M., Theuns, T., & Aguirre, A. 2010, MNRAS, 409, 132

TABLE 6
Ton S 180: Object Summary

ID	RA	DEC	B (mag)	R (mag)	S/G[a]	Area ($\square''$)	flg[b]	z
1	00:57:27.9	–22:25:12	9.86 ± 0.08	9.37 ± 0.06	0.69	253.5	0	···
2	00:56:52.8	–22:11:23	12.07 ± 0.08	11.42 ± 0.06	0.95	40.1	0	···
3	00:56:34.2	–22:29:02	15.35 ± 0.09	14.34 ± 0.06	1.00	3.5	0	···
4	00:56:33.8	–22:15:29	19.34 ± 0.10	17.53 ± 0.06	0.02	5.8	0	···
5	00:56:32.1	–22:31:34	21.96 ± 0.20	20.94 ± 0.10	0.82	3.3	0	···
6	00:56:32.0	–22:28:30	19.97 ± 0.11	18.10 ± 0.06	0.48	4.5	0	···
7	00:56:33.0	–22:11:44	19.09 ± 0.10	17.16 ± 0.06	0.88	5.0	0	···
8	00:56:32.4	–22:11:41	23.32 ± 0.54	21.59 ± 0.13	0.20	4.3	0	···
9	00:56:32.0	–22:24:37	21.65 ± 0.18	20.28 ± 0.08	0.12	3.9	0	···
10	00:56:32.6	–22:15:52	21.40 ± 0.15	20.02 ± 0.07	0.31	2.9	0	···

Note. — [The complete version of this table is in the electronic edition of the Journal. The printed edition contains only a sample.]

[a] Star/galaxy classifier calculated by SExtractor. Values near unity indicate a stellar-like point-spread function.

[b] This binary flag has the following code: 1: Survey target; 2: Spectrum taken; 4: Redshift measured.

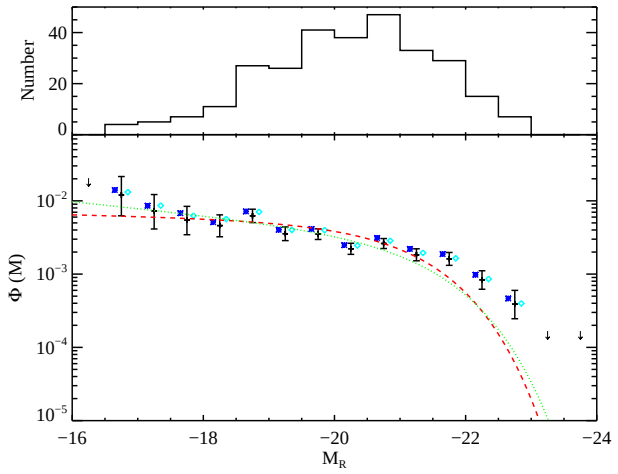


Fig. 41.— Luminosity function estimated from the 17 fields of the LCO/WFCCD survey that have greater than 70% completeness to 10′ from the quasar to $R \leq 19.5$ mag. Black points with error bars show the results without a correction for incompleteness and assume Poisson uncertainties based on the number of galaxies detected (upper panel). The blue stars and cyan diamonds show the estimated $\Phi(M)$ values after adopting magnitude-independent and dependent completeness corrections respectively (see the text for a full description). The dashed (red) and dotted (green) curves show the luminosity functions derived from the SDSS by Blanton et al. (2003) and Montero-Dorta & Prada (2009) respectively, corrected to our assumed cosmology ($h = 0.72$). The offset at high luminosity may be the result of an Eddington bias in our estimation of $\Phi(M)$ and/or a modest offset between our R-band photometry and the SDSS r-band measurements.

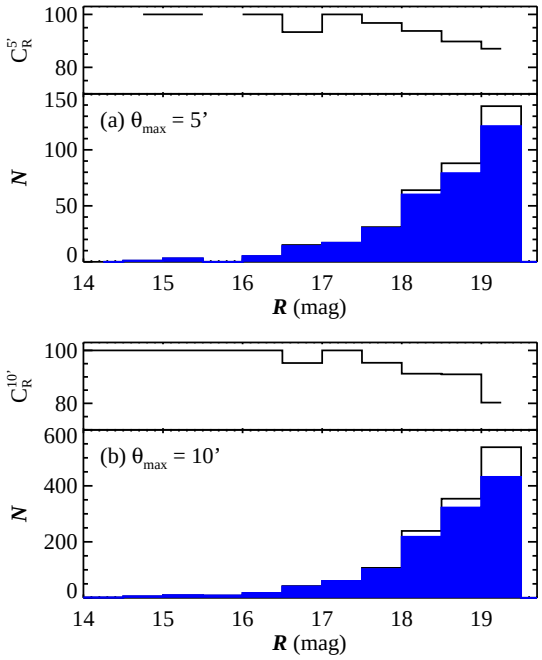


Fig. 42.— The lower plots of each panel show histograms of the targeted (open, black) and observed (solid, blue) galaxies in the 17 fields used to estimate the luminosity function (Figure 41). These histograms are shown for (a) $\theta_{\rm max} = 5'$ and (b) $\theta_{\rm max} = 10'$. In the upper plot of each panel, we show the completeness percentile C_R as a function of apparent magnitude. These values are used in the magnitude-dependent completeness correction of the luminosity function.

Williger, G. M., Heap, S. R., Weymann, R. J., Davé, R., Ellingson, E., Carswell, R. F., Tripp, T. M., & Jenkins, E. B. 2006, ApJ, 636, 631

TABLE 7
Ton S 210: Object Summary

ID	RA	DEC	B (mag)	R (mag)	S/G[a]	Area ($\square''$)	flg[b]	z
1	01:21:01.7	–28:14:24	16.10 ± 0.10	13.78 ± 0.06	1.00	4.7	0	···
2	01:21:00.1	–28:13:04	18.81 ± 0.09	17.36 ± 0.07	0.47	10.4	0	···
3	01:20:58.4	–28:13:53	19.05 ± 0.09	17.87 ± 0.07	0.13	4.9	0	···
4	01:20:56.6	–28:30:40	21.65 ± 0.23	18.85 ± 0.07	0.19	4.9	0	···
5	01:20:57.4	–28:22:13	19.54 ± 0.10	18.31 ± 0.07	0.02	6.9	0	···
6	01:20:57.7	–28:16:38	19.50 ± 0.09	18.63 ± 0.07	0.09	5.1	0	···
7	01:20:57.2	–28:21:14	20.68 ± 0.12	18.19 ± 0.07	0.99	2.1	0	···
8	01:20:57.1	–28:19:15	24.85 ± 1.70	21.36 ± 0.12	0.98	3.1	0	···
9	01:20:56.6	–28:23:16	22.62 ± 0.29	19.87 ± 0.07	0.99	1.9	0	···
10	01:20:55.9	–28:30:45	22.82 ± 0.43	20.35 ± 0.09	1.00	4.3	0	···

Note. — [The complete version of this table is in the electronic edition of the Journal. The printed edition contains only a sample.]

[a] Star/galaxy classifier calculated by SExtractor. Values near unity indicate a stellar-like point-spread function.

[b] This binary flag has the following code: 1: Survey target; 2: Spectrum taken; 4: Redshift measured.

TABLE 8
PKS0312-770: Object Summary

ID	RA	DEC	R (mag)	S/G[a]	Area ($\square''$)	flg[b]	z
1	03:11:42.7	–76:33:44	12.65 ± 0.01	1.00	7.2	0	···
2	03:12:28.6	–76:33:42	18.71 ± 0.02	0.12	10.2	0	···
3	03:12:10.2	–76:33:40	17.71 ± 0.01	1.00	4.6	0	···
4	03:14:33.7	–76:33:39	16.63 ± 0.01	1.00	4.6	0	···
5	03:12:34.0	–76:33:31	19.25 ± 0.03	0.85	3.8	0	···
6	03:11:25.3	–76:33:23	20.89 ± 0.08	0.12	7.8	0	···
7	03:12:52.6	–76:33:25	19.44 ± 0.03	0.56	5.2	0	···
8	03:10:19.9	–76:33:15	20.60 ± 0.10	0.98	2.7	0	···
9	03:13:01.0	–76:33:22	21.29 ± 0.12	1.00	5.5	0	···
10	03:14:36.7	–76:33:23	20.19 ± 0.05	0.97	8.1	0	···

Note. — [The complete version of this table is in the electronic edition of the Journal. The printed edition contains only a sample.]

[a] Star/galaxy classifier calculated by SExtractor. Values near unity indicate a stellar-like point-spread function.

[b] This binary flag has the following code: 1: Survey target; 2: Spectrum taken; 4: Redshift measured.

TABLE 9
PKS0558-504: Object Summary

ID	RA	DEC	B (mag)	R (mag)	S/G[a]	Area ($\square''$)	flg[b]	z
1	05:59:38.2	–50:18:33	10.41 ± 0.09	9.57 ± 0.06	0.69	149.9	0	···
2	05:59:20.5	–50:17:37	11.53 ± 0.09	10.80 ± 0.06	0.73	48.9	0	···
3	05:58:56.4	–50:27:28	12.41 ± 0.09	11.06 ± 0.06	0.75	38.3	0	···
4	05:58:48.3	–50:17:10	9.97 ± 0.09	9.98 ± 0.06	0.69	97.9	0	···
5	05:58:44.9	–50:24:12	10.51 ± 0.09	10.05 ± 0.06	0.69	94.4	0	···
6	05:58:45.6	–50:25:13	14.00 ± 0.09	13.27 ± 0.06	1.00	5.8	0	···
7	05:58:45.7	–50:16:04	12.78 ± 0.09	12.20 ± 0.06	1.00	14.2	0	···
8	05:58:39.9	–50:26:41	18.09 ± 0.09	17.13 ± 0.06	1.00	2.5	0	···
9	05:58:42.0	–50:26:33	12.30 ± 0.09	11.76 ± 0.06	0.98	20.0	0	···
10	05:58:43.5	–50:22:24	13.99 ± 0.09	13.12 ± 0.06	1.00	6.4	0	···

Note. — [The complete version of this table is in the electronic edition of the Journal. The printed edition contains only a sample.]

[a] Star/galaxy classifier calculated by SExtractor. Values near unity indicate a stellar-like point-spread function.

[b] This binary flag has the following code: 1: Survey target; 2: Spectrum taken; 4: Redshift measured.

TABLE 10
PG1004+130: Object Summary

ID	RA	DEC	B (mag)	R (mag)	S/G[a]	Area ($\square''$)	flg[b]	z
1	10:06:47.3	+12:46:52	8.19 ± 0.00	8.74 ± 0.00	0.69	217.7	0	···
2	10:06:57.9	+12:40:53	10.58 ± 0.00	11.13 ± 0.00	0.75	30.0	0	···
3	10:06:40.6	+12:47:50	21.44 ± 0.24	21.99 ± 0.24	1.00	2.4	0	···
4	10:06:39.5	+12:40:58	19.82 ± 0.06	20.37 ± 0.06	0.22	3.7	0	···
5	10:06:38.8	+12:37:14	17.74 ± 0.01	18.29 ± 0.01	1.00	2.6	0	···
6	10:06:40.1	+12:48:43	21.92 ± 0.30	22.46 ± 0.30	0.97	7.6	0	···
7	10:06:40.3	+12:51:47	17.97 ± 0.01	18.51 ± 0.01	1.00	2.5	0	···
8	10:06:39.4	+12:44:47	19.73 ± 0.07	20.28 ± 0.07	0.12	5.7	0	···
9	10:06:39.5	+12:45:04	21.60 ± 0.29	22.15 ± 0.29	0.35	9.2	0	···
10	10:06:38.5	+12:37:47	19.38 ± 0.05	19.93 ± 0.05	0.15	3.6	0	···

Note. — [The complete version of this table is in the electronic edition of the Journal. The printed edition contains only a sample.]

[a] Star/galaxy classifier calculated by SExtractor. Values near unity indicate a stellar-like point-spread function.

[b] This binary flag has the following code: 1: Survey target; 2: Spectrum taken; 4: Redshift measured.

TABLE 11
HE1029-140: Object Summary

ID	RA	DEC	B (mag)	R (mag)	S/G[a]	Area ($\square''$)	flg[b]	z
1	10:31:16.6	–14:21:26	14.12 ± 0.00	13.23 ± 0.00	1.00	6.2	0	···
2	10:31:15.3	–14:14:52	15.22 ± 0.00	13.97 ± 0.01	1.00	3.9	0	···
3	10:31:13.1	–14:15:55	16.15 ± 0.01	14.62 ± 0.01	1.00	2.6	0	···
4	10:31:13.4	–14:11:51	16.64 ± 0.01	15.80 ± 0.01	1.00	2.2	0	···
5	10:31:13.9	–14:06:06	18.95 ± 0.03	17.90 ± 0.01	0.87	6.1	7	0.13066
6	10:31:11.8	–14:21:00	16.48 ± 0.01	15.64 ± 0.00	1.00	2.8	0	···
7	10:31:12.5	–14:16:26	17.81 ± 0.01	16.50 ± 0.01	1.00	2.1	0	···
8	10:31:12.2	–14:13:53	19.50 ± 0.05	18.30 ± 0.02	0.28	4.9	7	0.19151
9	10:31:12.5	–14:11:37	20.58 ± 0.07	18.95 ± 0.02	0.98	2.6	7	−0.00008
10	10:31:12.6	–14:11:10	22.97 ± 0.45	20.40 ± 0.05	1.00	2.0	0	···

Note. — [The complete version of this table is in the electronic edition of the Journal. The printed edition contains only a sample.]

[a] Star/galaxy classifier calculated by SExtractor. Values near unity indicate a stellar-like point-spread function.

[b] This binary flag has the following code: 1: Survey target; 2: Spectrum taken; 4: Redshift measured.

TABLE 12
PG1116+215: Object Summary

ID	RA	DEC	B (mag)	R (mag)	S/G[a]	Area ($\square''$)	flg[b]	z
1	11:18:30.2	+21:17:08	18.76 ± 0.05	10.10 ± 0.03	0.98	125.2	0	···
2	11:18:29.2	+21:14:00	17.34 ± 0.01	15.64 ± 0.01	0.07	8.0	7	0.06038
3	11:18:25.4	+21:08:33	20.25 ± 0.05	19.17 ± 0.02	0.59	5.4	1	···
4	11:18:25.1	+21:18:15	23.88 ± 1.14	21.55 ± 0.14	0.22	14.2	0	···
5	11:18:25.9	+21:18:06	21.21 ± 0.18	19.83 ± 0.06	0.03	15.4	0	···
6	11:18:25.3	+21:16:13	23.11 ± 0.57	20.92 ± 0.10	0.08	12.8	0	···
7	11:18:24.9	+21:16:10	22.87 ± 0.59	20.75 ± 0.09	0.03	16.2	0	···
8	11:18:25.9	+21:16:25	20.53 ± 0.10	18.95 ± 0.03	0.03	12.2	0	···
9	11:18:26.9	+21:27:28	16.91 ± 0.01	15.06 ± 0.01	1.00	3.2	0	···
10	11:18:26.0	+21:27:25	21.56 ± 0.21	18.46 ± 0.01	0.99	4.5	1	···

Note. — [The complete version of this table is in the electronic edition of the Journal. The printed edition contains only a sample.]

[a] Star/galaxy classifier calculated by SExtractor. Values near unity indicate a stellar-like point-spread function.

[b] This binary flag has the following code: 1: Survey target; 2: Spectrum taken; 4: Redshift measured.

TABLE 13
PG1211+143: Object Summary

ID	RA	DEC	B (mag)	R (mag)	S/G[a]	Area ($\square''$)	flg[b]	z
1	12:14:00.7	+14:13:16	12.30 ± 0.09	10.94 ± 0.07	0.99	28.4	0	···
2	12:13:51.9	+14:13:23	16.04 ± 0.09	14.81 ± 0.07	0.03	35.2	0	···
3	12:13:58.3	+14:13:05	14.94 ± 0.09	13.93 ± 0.07	1.00	5.9	0	···
4	12:14:35.3	+14:13:44	25.76 ± 2.12	22.05 ± 0.12	0.98	2.5	0	···
5	12:14:29.6	+14:14:05	19.90 ± 0.10	17.77 ± 0.07	0.07	6.9	7	0.15545
6	12:13:42.4	+14:14:13	21.00 ± 0.11	19.93 ± 0.08	0.12	6.9	0	···
7	12:14:45.0	+14:13:57	21.25 ± 0.12	19.80 ± 0.07	0.13	4.8	0	···
8	12:14:28.2	+14:14:05	20.27 ± 0.10	18.88 ± 0.07	0.13	7.1	1	···
9	12:14:40.8	+14:14:01	19.92 ± 0.10	18.00 ± 0.07	0.78	7.2	1	···
10	12:14:40.9	+14:14:06	23.36 ± 0.32	21.58 ± 0.11	0.82	4.4	0	···

Note. — [The complete version of this table is in the electronic edition of the Journal. The printed edition contains only a sample.]

[a] Star/galaxy classifier calculated by SExtractor. Values near unity indicate a stellar-like point-spread function.

[b] This binary flag has the following code: 1: Survey target; 2: Spectrum taken; 4: Redshift measured.

TABLE 14
PG1216+069: Object Summary

ID	RA	DEC	B (mag)	R (mag)	S/G[a]	Area ($\square''$)	flg[b]	z
1	12:18:32.1	+06:32:29	28.60 ± 23.69	23.06 ± 0.41	1.00	1.6	0	···
2	12:18:38.6	+06:42:29	15.83 ± 0.00	14.86 ± 0.00	0.05	33.1	7	0.00667
3	12:18:35.1	+06:29:41	19.17 ± 0.05	18.07 ± 0.02	0.03	20.7	0	···
4	12:18:33.7	+06:28:08	24.86 ± 1.37	22.17 ± 0.14	0.96	3.1	0	···
5	12:18:33.7	+06:29:06	22.62 ± 0.25	20.61 ± 0.05	1.00	2.6	0	···
6	12:18:33.2	+06:40:52	19.86 ± 0.13	16.77 ± 0.02	0.03	57.2	0	···
7	12:18:33.6	+06:46:39	14.59 ± 0.00	13.99 ± 0.00	1.00	3.4	0	···
8	12:18:33.0	+06:34:06	20.03 ± 0.04	18.67 ± 0.02	0.99	3.4	0	···
9	12:18:33.4	+06:38:45	24.76 ± 1.82	21.16 ± 0.10	0.12	5.6	0	···
10	12:18:33.1	+06:40:30	22.14 ± 0.37	18.97 ± 0.04	0.03	16.6	0	···

Note. — [The complete version of this table is in the electronic edition of the Journal. The printed edition contains only a sample.]

[a] Star/galaxy classifier calculated by SExtractor. Values near unity indicate a stellar-like point-spread function.

[b] This binary flag has the following code: 1: Survey target; 2: Spectrum taken; 4: Redshift measured.

TABLE 15
3C273: Object Summary

ID	RA	DEC	B (mag)	R (mag)	S/G[a]	Area ($\square''$)	flg[b]	z
1	12:28:23.7	+02:09:17	26.82 ± 5.73	23.58 ± 0.25	1.00	3.5	0	···
2	12:28:22.2	+01:55:30	23.45 ± 0.35	21.95 ± 0.07	1.00	2.1	0	···
3	12:28:22.2	+01:55:01	22.74 ± 0.23	21.31 ± 0.05	1.00	2.1	0	···
4	12:28:22.1	+01:54:39	23.44 ± 0.35	22.18 ± 0.08	0.98	1.7	0	···
5	12:28:21.8	+01:51:53	23.13 ± 0.31	21.53 ± 0.05	1.00	1.9	0	···
6	12:28:23.7	+02:09:08	24.55 ± 1.24	22.21 ± 0.11	0.98	3.4	0	···
7	12:28:23.0	+02:02:25	24.95 ± 1.82	22.59 ± 0.16	0.15	2.9	0	···
8	12:28:23.1	+02:02:11	28.23 ± 14.61	23.70 ± 0.32	0.98	1.3	0	···
9	12:28:23.8	+02:08:12	25.41 ± 1.28	24.00 ± 0.35	0.98	1.5	0	···
10	12:28:23.5	+02:05:35	24.12 ± 0.86	22.17 ± 0.13	0.90	5.6	0	···

Note. — [The complete version of this table is in the electronic edition of the Journal. The printed edition contains only a sample.]

[a] Star/galaxy classifier calculated by SExtractor. Values near unity indicate a stellar-like point-spread function.

[b] This binary flag has the following code: 1: Survey target; 2: Spectrum taken; 4: Redshift measured.

TABLE 16
Q1230+095: Object Summary

ID	RA	DEC	B (mag)	R (mag)	S/G[a]	Area ($\square''$)	flg[b]	z
1	12:33:53.8	+09:31:53	11.39 ± 0.01	9.17 ± 0.01	0.69	217.9	0	···
2	12:32:44.9	+09:39:38	11.28 ± 0.00	10.81 ± 0.00	0.72	46.6	0	···
3	12:32:44.6	+09:22:05	17.48 ± 0.01	16.13 ± 0.01	0.01	8.5	7	0.11526
4	12:32:42.9	+09:20:40	19.51 ± 0.06	18.59 ± 0.03	0.03	12.2	1	···
5	12:32:44.0	+09:30:56	17.58 ± 0.01	16.02 ± 0.01	1.00	2.8	0	···
6	12:32:43.0	+09:24:56	18.57 ± 0.02	16.88 ± 0.01	1.00	2.6	0	···
7	12:32:42.9	+09:27:53	22.81 ± 0.45	20.24 ± 0.05	0.57	2.5	0	···
8	12:32:43.6	+09:35:56	21.20 ± 0.13	19.57 ± 0.04	0.18	2.9	0	···
9	12:32:41.8	+09:20:56	18.48 ± 0.02	16.35 ± 0.01	1.00	4.6	0	···
10	12:32:43.6	+09:36:08	22.53 ± 0.37	20.08 ± 0.05	0.40	3.0	0	···

Note. — [The complete version of this table is in the electronic edition of the Journal. The printed edition contains only a sample.]

[a] Star/galaxy classifier calculated by SExtractor. Values near unity indicate a stellar-like point-spread function.

[b] This binary flag has the following code: 1: Survey target; 2: Spectrum taken; 4: Redshift measured.

TABLE 17
PKS1302-102: Object Summary

ID	RA	DEC	B (mag)	R (mag)	S/G[a]	Area ($\square''$)	flg[b]	z
1	13:05:43.7	–10:30:07	10.28 ± 0.00	8.93 ± 0.01	0.69	334.3	0	···
2	13:04:57.9	–10:25:47	13.20 ± 0.00	12.36 ± 0.00	1.00	13.8	0	···
3	13:04:57.8	–10:26:05	17.48 ± 0.02	15.15 ± 0.01	1.00	3.2	0	···
4	13:04:56.0	–10:29:18	20.06 ± 0.11	18.11 ± 0.02	0.09	6.8	7	0.27252
5	13:04:54.6	–10:39:58	18.85 ± 0.04	17.89 ± 0.01	0.13	4.6	7	0.04576
6	13:04:54.9	–10:33:57	17.45 ± 0.01	15.92 ± 0.01	1.00	2.3	0	···
7	13:04:56.1	–10:25:29	23.12 ± 0.78	20.75 ± 0.08	0.98	1.9	0	···
8	13:04:55.0	–10:32:28	21.53 ± 0.25	19.65 ± 0.04	0.13	3.7	0	···
9	13:04:56.0	–10:21:04	20.36 ± 0.11	18.71 ± 0.02	0.15	3.6	1	···
10	13:04:55.1	–10:29:17	19.09 ± 0.03	18.13 ± 0.01	0.98	3.4	0	···

Note. — [The complete version of this table is in the electronic edition of the Journal. The printed edition contains only a sample.]

[a] Star/galaxy classifier calculated by SExtractor. Values near unity indicate a stellar-like point-spread function.

[b] This binary flag has the following code: 1: Survey target; 2: Spectrum taken; 4: Redshift measured.

TABLE 18
PG1307+085: Object Summary

ID	RA	DEC	B (mag)	R (mag)	S/G[a]	Area ($\square''$)	flg[b]	z
1	13:09:49.7	+08:11:05	11.72 ± 0.00	10.34 ± 0.01	0.69	84.1	0	···
2	13:09:08.0	+08:09:16	13.90 ± 0.00	13.12 ± 0.00	1.00	6.7	0	···
3	13:09:07.3	+08:09:35	20.00 ± 0.09	14.10 ± 0.02	1.00	4.8	0	···
4	13:09:09.7	+08:27:13	22.33 ± 0.33	20.41 ± 0.06	0.13	3.3	0	···
5	13:09:09.5	+08:27:09	21.29 ± 0.16	20.35 ± 0.07	0.15	5.2	0	···
6	13:09:07.9	+08:11:41	17.33 ± 0.01	16.59 ± 0.01	1.00	2.3	0	···
7	13:09:09.1	+08:23:48	17.21 ± 0.01	16.48 ± 0.01	1.00	2.3	0	···
8	13:09:09.6	+08:28:56	17.98 ± 0.01	16.94 ± 0.01	1.00	2.2	0	···
9	13:09:07.6	+08:09:48	23.62 ± 1.08	20.83 ± 0.10	0.20	5.1	0	···
10	13:09:09.5	+08:27:53	24.44 ± 1.45	20.89 ± 0.07	0.99	1.8	0	···

Note. — [The complete version of this table is in the electronic edition of the Journal. The printed edition contains only a sample.]

[a] Star/galaxy classifier calculated by SExtractor. Values near unity indicate a stellar-like point-spread function.

[b] This binary flag has the following code: 1: Survey target; 2: Spectrum taken; 4: Redshift measured.

TABLE 19
MRK1383: Object Summary

ID	RA	DEC	B (mag)	R (mag)	S/G[a]	Area ($\square''$)	flg[b]	z
1	14:29:00.6	+01:26:39	10.44 ± 0.00	9.62 ± 0.00	0.69	140.4	0	···
2	14:28:57.4	+01:24:05	11.17 ± 0.00	10.52 ± 0.00	0.73	60.6	0	···
3	14:28:29.6	+01:07:36	12.80 ± 0.01	11.16 ± 0.01	0.87	34.0	0	···
4	14:28:21.9	+01:06:47	18.66 ± 0.04	17.19 ± 0.01	0.01	6.3	1	···
5	14:28:21.3	+01:06:46	23.57 ± 0.82	21.66 ± 0.13	0.98	2.4	0	···
6	14:28:24.2	+01:27:37	20.25 ± 0.09	18.02 ± 0.01	1.00	2.4	0	···
7	14:28:24.2	+01:27:51	22.63 ± 0.54	20.90 ± 0.10	0.12	2.9	0	···
8	14:28:23.2	+01:18:37	22.68 ± 0.57	19.94 ± 0.05	0.99	2.5	0	···
9	14:28:23.7	+01:26:27	22.09 ± 0.30	20.53 ± 0.07	0.93	2.5	0	···
10	14:28:24.0	+01:28:01	22.26 ± 0.37	19.38 ± 0.03	0.98	2.1	0	···

Note. — [The complete version of this table is in the electronic edition of the Journal. The printed edition contains only a sample.]

[a] Star/galaxy classifier calculated by SExtractor. Values near unity indicate a stellar-like point-spread function.

[b] This binary flag has the following code: 1: Survey target; 2: Spectrum taken; 4: Redshift measured.

TABLE 20
Q1553+113: Object Summary

ID	RA	DEC	B (mag)	R (mag)	S/G[a]	Area ($\square''$)	flg[b]	z
1	15:55:06.9	+11:14:54	12.14 ± 0.00	11.18 ± 0.00	0.96	30.4	0	···
2	15:55:00.4	+10:59:45	18.57 ± 0.05	17.24 ± 0.02	0.17	23.0	0	···
3	15:55:02.2	+10:59:33	17.53 ± 0.02	16.71 ± 0.01	0.03	22.3	0	···
4	15:55:00.7	+11:04:26	16.22 ± 0.01	14.89 ± 0.01	0.02	15.4	7	0.04052
5	15:54:57.8	+11:01:35	22.80 ± 0.67	19.64 ± 0.04	0.20	3.0	1	···
6	15:54:58.5	+11:19:32	17.09 ± 0.01	15.82 ± 0.01	1.00	2.5	0	···
7	15:54:58.2	+11:17:38	16.57 ± 0.01	15.40 ± 0.01	1.00	2.6	0	···
8	15:54:58.1	+11:21:23	21.30 ± 0.15	19.22 ± 0.02	0.99	2.4	0	···
9	15:54:57.6	+11:21:27	22.22 ± 0.39	20.12 ± 0.06	0.12	3.8	0	···
10	15:54:56.3	+11:05:18	22.28 ± 0.29	20.62 ± 0.06	0.98	2.1	0	···

Note. — [The complete version of this table is in the electronic edition of the Journal. The printed edition contains only a sample.]

[a] Star/galaxy classifier calculated by SExtractor. Values near unity indicate a stellar-like point-spread function.

[b] This binary flag has the following code: 1: Survey target; 2: Spectrum taken; 4: Redshift measured.

TABLE 21
PKS2005-489: Object Summary

ID	RA	DEC	B (mag)	R (mag)	S/G[a]	Area ($\square''$)	flg[b]	z
1	20:09:57.0	–48:39:37	24.07 ± 0.55	22.75 ± 0.14	0.98	3.0	0	···
2	20:10:27.4	–48:39:42	25.30 ± 9.99	23.33 ± 0.22	0.97	1.7	0	···
3	20:10:18.0	–48:39:41	25.25 ± 9.99	23.47 ± 0.26	0.97	3.7	0	···
4	20:10:11.1	–48:39:40	25.20 ± 2.48	20.77 ± 0.07	0.99	2.5	0	···
5	20:10:17.0	–48:39:44	24.47 ± 0.97	22.50 ± 0.14	0.98	3.9	0	···
6	20:09:45.5	–48:39:37	21.46 ± 0.13	20.35 ± 0.07	0.98	2.6	0	···
7	20:09:10.9	–48:39:36	26.00 ± 2.54	23.67 ± 0.24	0.96	1.7	0	···
8	20:09:19.3	–48:39:37	24.66 ± 0.93	23.31 ± 0.22	0.97	2.6	0	···
9	20:09:23.9	–48:39:32	22.53 ± 0.33	20.48 ± 0.07	0.82	3.7	0	···
10	20:10:22.2	–48:39:49	23.53 ± 0.46	22.03 ± 0.11	1.00	2.5	0	···

Note. — [The complete version of this table is in the electronic edition of the Journal. The printed edition contains only a sample.]

[a] Star/galaxy classifier calculated by SExtractor. Values near unity indicate a stellar-like point-spread function.

[b] This binary flag has the following code: 1: Survey target; 2: Spectrum taken; 4: Redshift measured.

TABLE 22
FJ2155-092: Object Summary

ID	RA	DEC	B (mag)	R (mag)	S/G[a]	Area ($\square''$)	flg[b]	z
1	21:54:16.5	–09:20:36	13.37 ± 0.09	11.93 ± 0.06	1.00	19.4	0	···
2	21:54:15.7	–09:29:17	16.32 ± 0.09	14.94 ± 0.06	0.68	9.7	0	···
3	21:54:13.4	–09:14:10	15.51 ± 0.09	14.55 ± 0.06	1.00	3.2	0	···
4	21:54:12.0	–09:23:15	13.41 ± 0.09	12.65 ± 0.06	1.00	10.3	0	···
5	21:54:12.0	–09:12:53	20.31 ± 0.15	18.05 ± 0.07	0.22	3.8	0	···
6	21:54:11.6	–09:12:54	24.50 ± 2.61	21.14 ± 0.14	0.13	4.8	0	···
7	21:54:11.4	–09:20:01	20.78 ± 0.14	19.03 ± 0.07	0.99	2.3	0	···
8	21:54:11.1	–09:18:56	20.04 ± 0.14	17.71 ± 0.07	0.22	4.1	0	···
9	21:54:11.0	–09:19:03	21.20 ± 0.19	18.50 ± 0.07	0.99	2.5	0	···
10	21:54:11.5	–09:15:46	19.16 ± 0.10	17.82 ± 0.06	1.00	2.5	0	···

Note. — [The complete version of this table is in the electronic edition of the Journal. The printed edition contains only a sample.]

[a] Star/galaxy classifier calculated by SExtractor. Values near unity indicate a stellar-like point-spread function.

[b] This binary flag has the following code: 1: Survey target; 2: Spectrum taken; 4: Redshift measured.

TABLE 23
PKS2155-304: Object Summary

ID	RA	DEC	B (mag)	R (mag)	S/G[a]	Area ($\square''$)	flg[b]	z
1	21:59:04.0	–30:09:30	9.80 ± 0.08	9.27 ± 0.06	0.69	265.2	0	···
2	21:58:12.6	–30:17:46	12.89 ± 0.08	12.00 ± 0.06	0.99	21.0	0	···
3	21:58:11.4	–30:19:08	15.88 ± 0.09	14.82 ± 0.06	0.03	22.0	7	0.04528
4	21:58:08.2	–30:11:58	13.55 ± 0.09	12.33 ± 0.06	1.00	15.6	0	···
5	21:58:02.3	–30:15:35	15.22 ± 0.08	14.49 ± 0.06	1.00	3.1	0	···
6	21:58:03.0	–30:06:04	19.50 ± 0.12	17.12 ± 0.06	0.04	6.3	0	···
7	21:58:00.3	–30:19:49	20.61 ± 0.14	18.30 ± 0.06	0.89	3.7	0	···
8	21:58:01.8	–30:02:37	21.55 ± 0.20	19.17 ± 0.07	0.48	4.0	0	···
9	21:58:00.8	–30:07:21	21.61 ± 0.18	19.21 ± 0.07	1.00	2.4	0	···
10	21:57:59.4	–30:21:38	19.98 ± 0.09	18.80 ± 0.06	0.98	2.1	0	···

Note. — [The complete version of this table is in the electronic edition of the Journal. The printed edition contains only a sample.]

[a] Star/galaxy classifier calculated by SExtractor. Values near unity indicate a stellar-like point-spread function.

[b] This binary flag has the following code: 1: Survey target; 2: Spectrum taken; 4: Redshift measured.